NASA TECHNICAL NOTE

NASA TN D-8303

A COMPUTER SIMULATION OF THE AFTERBURNING PROCESSES OCCURRING WITHIN SOLID ROCKET MOTOR PLUMES IN THE TROPOSPHERE

Richard I. Gomberg and Roger B. Stewart

Langley Research Center
Hampton, Va. 23665

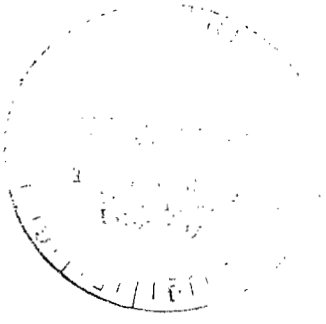

NATIONAL AERONAUTICS AND SPACE ADMINISTRATION • WASHINGTON, D. C. • DECEMBER 1976

1. Report No.	2. Government Accession No.	3. Recipient's Catalog No.
NASA TN D-8303		

4. Title and Subtitle	5. Report Date
A COMPUTER SIMULATION OF THE AFTERBURNING PROCESSES OCCURRING WITHIN SOLID ROCKET MOTOR PLUMES IN THE TROPOSPHERE	December 1976
	6. Performing Organization Code
7. Author(s)	8. Performing Organization Report No.
Richard I. Gomberg and Roger B. Stewart	L-10964
	10. Work Unit No. 197-40-02-01
9. Performing Organization Name and Address	11. Contract or Grant No.
NASA Langley Research Center Hampton, VA 23665	
	13. Type of Report and Period Covered
12. Sponsoring Agency Name and Address	Technical Note
National Aeronautics and Space Administration Washington, DC 20546	14. Sponsoring Agency Code

15. Supplementary Notes

16. Abstract

As part of a continuing study of the environmental effects of solid rocket motor (SRM) operations in the troposphere, a numerical model is used to simulate the afterburning processes occurring in solid rocket motor plumes and to predict the quantities of potentially harmful chemical species which are created. The calculations include the effects of finite-rate chemistry and turbulent mixing. It is found that the amount of NO produced is much less than the amount of HCl present in the plume, that chlorine will appear predominantly in the form of HCl although some molecular chlorine is present, and that combustion is complete as is evident from the predominance of carbon dioxide over carbon monoxide.

17. Key Words (Suggested by Author(s))	18. Distribution Statement
Environmental effects of space shuttle Afterburning Troposphere Solid rocket motors	Unclassified - Unlimited Subject Category 45

19. Security Classif. (of this report)	20. Security Classif. (of this page)	21. No. of Pages	22. Price*
Unclassified	Unclassified	41	$3.75

* For sale by the National Technical Information Service, Springfield, Virginia 22161

A COMPUTER SIMULATION OF THE AFTERBURNING PROCESSES OCCURRING WITHIN SOLID ROCKET MOTOR PLUMES IN THE TROPOSPHERE

Richard I. Gomberg and Roger B. Stewart
Langley Research Center

SUMMARY

As part of a continuing study of the environmental effects of solid rocket motor (SRM) operations in the troposphere, a numerical model is used to simulate the afterburning processes occurring in solid rocket motor plumes and to predict the quantities of potentially harmful chemical species which are created. The calculations include the effects of finite-rate chemistry and turbulent mixing. It is found that the amount of NO produced is much less than the amount of HCl present in the plume, that chlorine will appear predominantly in the form of HCl although some molecular chlorine is present, and that combustion is complete as is evident from the predominance of carbon dioxide over carbon monoxide.

INTRODUCTION

This is the second in a series of papers dealing with chemical species released into the troposphere as a result of solid rocket motor operations. Reference 1 (NASA TN D-8137) dealt primarily with NO production from the space shuttle and Titan III-C solid motors. The present study expands the scope of investigation to include the partitioning of chlorine between the compounds HCl, Cl, Cl_2, and ClO. In addition, the partitioning of carbon between CO and CO_2 is considered, as well as the production of NO and NO_2.

The primary analytical tool used in the investigation was the low-altitude plume program, the LAPP code. (See ref. 2.) This computer program models the plume as axisymmetric, reacting concentric streamtubes with turbulent mixing between tubes. It is suitable for relatively low-altitude computational studies of afterburning in rocket plumes. Above an altitude of 15 km, the rocket nozzle flow becomes increasingly underexpanded and a shock pattern develops in the plume that is not accounted for by the code. The section that follows describes how the LAPP program is used in the present study as well as a modification which can be used to strengthen weaknesses in the model. Subsequent sections give estimates of the nitrogen, chlorine, and carbon-containing species which result from afterburning at various altitudes.

SYMBOLS

A area of plume, m^2

B activation energy

M	Mach number
n	real number
p	pressure
R	gas constant
r	effective nozzle-exit radius (derived from true exit radius by means of an isentropic expansion)
T	temperature
U	velocity of particle within plume
U_{av}	average velocity of particles within plume approaches
x	distance downstream of nozzle-exit plane, m
y	distance measured from center line of plume perpendicular to downstream direction
ρ	density of plume

Subscripts:

e	pertaining to exit plane of nozzle
Al_2O_3	pertaining to Al_2O_3
x	pertaining to a distance x (meters) downstream of exit plane

ANALYTICAL TECHNIQUES

The LAPP Program

Figure 1 is a diagram of a typical low-altitude rocket plume. The LAPP code used to model this plume is a time-independent axisymmetric model that divides the hydrodynamic flow field into streamtubes. The model is formulated in streamtube coordinates. The unperturbed atmosphere or free-stream flow is the outermost streamtube; the remaining streamtubes contain the plume. In each streamtube the governing differential equations are the reacting boundary-layer equations. (See ref. 3.) The numerical scheme used to solve these equations is mixed explicit-implicit.

Several eddy-viscosity models are presently available which describe the turbulent entrainment of air into the plume. The Donaldson-Gray model (ref. 4) was used in this investigation because of its success in prior studies by other investigators (ref. 5).

As inputs to the code, it is necessary to specify the conditions at the nozzle-exit plane (such as velocity, temperature, and composition of the exhaust gases), conditions in the unperturbed atmosphere, the chemical reactions to be considered, and all the pertinent thermochemical data. The nozzle-exit plane conditions for the space shuttle solid rocket motor (SRM) were furnished by Marshall Space Flight Center and the data for the Titan III-C SRM by Aerospace Corporation. (See tables I and II.) The unperturbed atmospheric conditions were taken from U.S. Standard Atmosphere (ref. 6); thermochemical data were taken from the JANNAF reports (ref. 7); and chemical reaction rate coefficients were taken from references 8 to 13.

Calculations were made for the shuttle SRM at altitudes of 0.7, 6, 10, and 15 km and for the Titan at altitudes of 0.9 and 18 km. At high altitudes the pressure of the gases at the exit plane is on the order of 1 atmosphere, whereas the ambient pressure is about 0.1 atmosphere. (1 atmosphere = 101.3 kPa.) For these high altitudes, a hand-calculated isentropic expansion is used to gain effective nozzle-exit plane conditions. This approach was used for the shuttle motor at 6, 10, and 15 km and for the Titan at 18 km. The chemical composition at the effective nozzle-exit plane was assumed to be identical to those of tables I and II. By using the mass flow rates taken from reference 14 and the isentropic assumption, the complete set of effective nozzle-exit plane conditions necessary to start the code at these higher altitudes are given in table III.

Because the reaction mechanism used in the code is not appropriate for temperatures below 600 K, the code cuts off all chemical kinetic reactions below this temperature. At all altitudes between sea level and 15 km, both the shuttle and Titan motors produce regions extending at least 0.5 km downstream of the nozzle-exit plane in which temperatures are well above 600 K.

The chemical reactions and the rate coefficients used in this study are given in table IV. These reactions are descriptive of processes occurring above 600 K. Although they are chemically inert in this model, certain species such as Al_2O_3 are considered because of their importance in maintaining a heat balance. These species are listed at the end of table IV. All constituents of the plume are taken to be ideal gases.

Mass Conservation

As was shown in reference 1, the LAPP code does not conserve mass. This effect is demonstrated in figure 2, which plots the mass flow of the inert species Al_2O_3 against downstream distance in the plume of a shuttle solid rocket motor at an altitude of 15 km. Since Al_2O_3 is inert and the code is time-independent, this quantity should be conserved. If x is the distance downstream, the mass flow rate of Al_2O_3 is $(\rho UA)_{Al_2O_3}$. This quantity should be constant for all x. As can be seen from figure 2, the quantity actually decreases with downstream distance.

Several calculations with variation in step size demonstrated that the problem is not a straightforward roundoff error as the mass loss was insensi-

tive to the step size used. The problem appears to be connected with the way the model allows the plume to spread out. In LAPP, the outermost streamtube is the unperturbed atmosphere which is taken to be a mixture of N_2 and O_2 only. At the atmospheric boundary the code truncates any constituents in the plume such as Al_2O_3, HCl, NO, etc. Thus, if the computational mesh is not allowed to spread as rapidly as the mass is viscously mixing outward, mass will in effect be lost by leaking out of the edges of the flow field.

The mechanism for expanding the plume in the LAPP code is the addition of streamtubes. Thus, it is important to add streamtubes at a proper rate to account for the expansion of the plume and to satisfy the nonleakage boundary condition. In the unmodified version of the code, streamtubes are added whenever the outermost tube (the unperturbed atmosphere) and its adjacent tube satisfy either

$$\frac{|U_{outer} - U_{adjacent}|}{|U_{outer}|} > 0.01$$

or

$$\frac{|U_{outer} - T_{adjacent}|}{|T_{outer}|} > 0.05$$

By varying the numbers which the inequalities must satisfy, one can control the rate of expansion of the flow field. At distances close to the nozzle-exit plane, the inequalities as they are stated seem to be adequate to satisfy the necessary boundary conditions. At distances far downstream, roughly greater than 250 m, the inequalities are too steep to allow the plume to expand properly in this region. A modification that can be made, then, is to lower the inequalities necessary to add streamtubes far downstream. The amount of lowering is easily determined by keeping careful track of $\left(|\rho UA|_{Al_2O_3}\right)_e \Big/ \left(|\rho UA|_{Al_2O_3}\right)_x$. By choosing inequalities so that the resultant expansion causes this ratio to stay close to one, the model will satisfy the nonleakage boundary condition.

Mass Conservation in Present Studies of Solid Booster Motor Plumes

By making use of the modified criteria stated previously, the mass loss due to "leakage" can be held to a few percent. Consider, for example, figure 2(a) in which is plotted the mass flow of Al_2O_3 against downstream distance for a shuttle SRM at an altitude of 15 km. As can be seen in contrast to that behavior in figure 2(b) by carefully controlling the expansion of the plume, the mass flow oscillates with small amplitude about the conserved value. In figure 3, the mass flow of Al_2O_3 for a shuttle motor at an altitude of 5 km is plotted as a function of downstream distance. Again, the mass loss is seen to be small. For each case studied, a careful analysis of the mass flow rate of inert species using the techniques described here was carried out in order to investigate possible mass losses. All calculations performed in this study were taken to a

distance of 1 km downstream of the exit plane. A reliable indicator of how closely mass is being conserved is obtained by comparing the mass flow of Al_2O_3 at a distance of 1 km downstream of the exit plane with the mass flow at the exit plane. In table V such a comparison is made for the various cases already described.

A Sensitivity Study

In addition to calculating the behavior of the afterburning plume for the cases already described, an attempt was made to determine the sensitivity of the model to variations in the input parameters. In particular, chemical reaction rates are not known precisely, but have associated with them uncertainties which can be as high as a factor of a thousand. Eddy diffusion coefficients are also quantities which are not known with great precision. A variation in a rate coefficient will cause variation of the resultant chemical composition of the plume. However, if the change in composition is small even when the rate coefficient is varied over its full range of experimental uncertainties, then the composition is said to be insensitive to uncertainties in the rate coefficient. To understand how sensitive this particular calculation is to experimental uncertainties in the rate coefficients, a series of computer simulations with varied rate coefficients were run of the afterburning from a shuttle SRM at an altitude of 10 km.

In each of the cases in this sensitivity study, identical nozzle-exit plane conditions appropriate to the shuttle SRM at 10 km were used. The chemical scheme, however, is changed several times to investigate the uncertainties in rate coefficients in some important reactions. Consider, for example, table VI. Of the 36 reactions used in the chemical scheme, 12 directly include the chlorine atom. The forward kinetic rates associated with these reactions are made to vary in one simulation as shown in the first column of table VI. All rate coefficients used in this model are of the form

$$\text{Rate coefficient} = CT^n \exp \frac{B}{RT}$$

where C is a constant and B is the activation energy. In the first column of table VI, new values for C are used for the 12 reactions shown. In the simulation, only these rate coefficients are varied; all other rates remain as shown in table IV.

In the next simulation, the rate coefficients shown in the second column were used. These variations cause all reactions producing atomic chlorine to be accelerated (first column) in the first simulation and slowed (second column) in the next simulation.

In table VII a similar study is made for atomic oxygen. One set of rate coefficients enhances O production, another set suppresses O production. In table VIII a set of rate coefficients speeding the combustion processes (within experimental uncertainties, of course) are used. In all cases, only the rate

coefficients shown are varied. As will be shown in detail, the model is fairly insensitive to the uncertainties in the chemical rate coefficients.

To study the effect of variations in turbulent mixing, a case is run with a different mixing model. A good alternate to Donaldson-Gray is the Ting-Libby model (ref. 15) which is used in this last case of the sensitivity study.

In each of the sensitivity study computer simulations, the conservation of mass was closely watched. As shown in table V, mass is conserved fairly accurately in these runs also.

RESULTS AND DISCUSSION

Calculations were made for a Titan solid propellant booster at 0.9 km and 18 km, and a shuttle motor at 0.7, 6, 10, and 15 km with sensitivity calculations at 10 km. These studies neglect the shock structure present in the plume and introduce some uncertainties, particularly at high altitudes. With increasing x/r, the temperatures in the plume decrease, the chemical reactions begin to slow down, and the velocities decrease. As x/r approaches the value where the center-line temperature drops below 600 K, chemical reactions are shut off in the model. Although the plume will continue to diffuse and therefore the absolute concentration of each specie will decrease with increasing x/r, the total mass flow of each specie crossing a plane perpendicular to x will be constant in this region (within the mass conservation limits previously described).

Farther downstream, the average velocity of the particles in the plume approaches ambient velocity. (All calculations are carried out in the frame of reference of the nozzle exit plane.) Thus, not only is the mass flow $(\rho U_{av} A)_x$ constant, but also

$$\frac{(\rho U_{av} A)_x}{(U_{av})_x} \longrightarrow (\rho A)_x \longrightarrow \text{Constant}$$

The physical meaning of $(\rho A)_x$ is that quantity of mass in a slab, the dimensions of which are equal to the area of the plume whose plane is perpendicular to x and whose length is 1 m in the x-direction. The value of $(\rho A)_x$ for a given species for large x is a reasonable indication of the quantity of that species that is deposited in the atmosphere. The unit of $(\rho A)_x$ is g/m.

NO Production in Solid Booster Motor Plumes

Table IX lists the production levels of NO and NO_2 for the various cases previously described. There are a number of interesting features in these results. At altitudes below 6 km, the shuttle booster produces roughly twice the NO of the Titan booster. This is quite reasonable since the two motors are

similar and the mass flow of the shuttle is roughly twice that of the Titan. At the high altitude of 18 km, however, in spite of the larger mass flow of the shuttle, the Titan SRM produces roughly twice the NO of the shuttle at an altitude of 15 km. As discussed in reference 1, this difference is due to the existence of a thrust-vector control system present in the Titan, but not in the shuttle. The thrust-vector control system consists of a tank of N_2O_4 which is strapped onto each booster and which is bled into the chamber through a series of steering jets in order to make fine course adjustments. In the high temperatures present in the chamber, much of the N_2O_4 breaks down into NO as well as O and O_2.

The effects of uncertainties in the rate coefficients on the production of NO are inherent in the results of the parametric studies of the shuttle at 10 km. The rate coefficients that are being used as best estimates result in a $(\rho A)_x$ of NO of 25 g/m at large x. However, when some of the uncertainties of the rate coefficients are put into the calculations, the result is that this NO production can be as low as a $(\rho A)_x$ of 21 g/m or as high as 37 g/m for large x.

By using the Ting-Libby viscosity model instead of the Donaldson-Gray model, the code predicts that oxygen is entrained into the plume at a more rapid rate than Donaldson-Gray predicts. This condition causes the combination of nitrogen and oxygen to occur at higher temperatures and over a longer period of time. Correspondingly, the NO levels rise to 41 g/m from 25 g/m.

The NO levels can be seen in some detail in figure 4. The quantity of NO and various other species in the plume in units of g/m is plotted as a function of downstream distance for the shuttle motor at 10 km. Results for both the Donaldson-Gray and Ting-Libby models are shown. For both models the quantity of Al_2O_3 as a function of downstream distance is very close. For the Donaldson-Gray model the NO production can be seen to rise to an asymptotic value of 31 g/m whereas it rises to a value of 41 g/m for the Ting-Libby case. Note that for the Ting-Libby case, the NO levels rise more rapidly than for the Donaldson-Gray case in the early parts of the plume where T is higher.

Chlorine Partitioning in Solid Booster Motor Plumes

Table X shows how chlorine is partitioned among HCl, Cl_2, and ClO in the various situations discussed. In all cases the plume partitions chlorine in amounts by weight of roughly 89 percent HCl, 9 percent Cl_2, and about 2 percent is in the form of Cl or ClO. By mole fraction HCl makes up more than 9 percent of the reacting chlorine-containing compounds in the plume. The shuttle plume will also contain some nonreacting particles such as AlCl and $AlCl_2$.

This partitioning of the reacting chlorine compounds is true for both the Titan and shuttle motors. In figure 5, $(\rho A)_x$ of various chlorine-containing species are plotted against downstream distance for a Titan motor at 0.9 km. In figure 6 a similar plot is made for a shuttle motor at an altitude of 5 km. In both cases as is the case at other altitudes, the partitioning of chlorine follows the pattern described.

Completeness of Combustion in Solid Booster Motor Plumes

The completeness of combustion can be discerned from the ratio of CO_2 to CO. At the exit plane of the Titan, there is a 9 to 1 ratio in g/m of CO to g/m of CO_2. For the shuttle motor there is a 7 to 1 ratio of CO to CO_2 at the exit plane. By the time afterburning is complete (at approximately 1 km downstream), much of the CO has combined with oxygen to form CO_2. The extent to which CO_2 has been created at the expense of CO is a good indication as to how complete the combustion is in the plume. From table XI it is clear that the combustion is almost total. Ratios of CO_2 to CO of a 100 to 1 are typical of the afterburned products.

The process of converting CO to CO_2 for a Titan motor is shown in figures 7 and 8. Figure 7 shows $(\rho A)_x$ in g/m of various species against downstream distance in the plume of a Titan motor at 0.9 km. As can be seen from figure 7, at the exit plane CO is the predominant species, but as a result of afterburning, CO_2 becomes by far the more prevalent quantity by the time the asymptotic region has been reached. In figure 8 is plotted the mole fraction of several species along the center line of the plume against downstream distance, again for the Titan at 0.9 km. Here again, the conversion of CO to CO_2 can be seen as the CO curve falls off rapidly when afterburning sets in and the mole fraction of CO_2 increases at the expense of the amount of CO present.

In figures 9 and 10 a similar set of curves is shown for the shuttle at 6 km. Both for $(\rho A)_x$ of species (fig. 9) and for the center-line mole fraction curves (fig. 10), the conversion of CO to CO_2 is easily seen.

Composition and Physical Characteristics

Figures 11 to 20 present a detailed analysis of the composition and physical characteristics of the plume of a shuttle motor at 0.7 km and at 15 km. Figures 11 to 13 describe $(\rho A)_x$ (in g/m). Notice that the $(\rho A)_x$ of "combustion" species produced at 0.7 km (fig. 11) are much greater than those at 15 km. This difference is due to the following condition: (1) the mass flow at the exit plane is smaller at 15 km than that at 0.7 km (ref. 14), (2) the free-stream velocity at 15 km is much greater than that at 0.7 km, and (3) the free-stream pressure at 15 km is less than that at 0.7 km.

In figure 12, quantities of chlorine-containing species $(\rho A)_x$ are plotted as a function of downstream distance for the 0.7- and 1.5-km shuttle motors. These figures show the partitioning of chlorine among the various species, whereas figure 13 concentrates on oxides of nitrogen.

Figures 14 to 16 show for the same conditions and species as figures 11 to 13, the behavior of the mole fraction along the center line plotted against downstream distance. In these figures it is seen that the mole fractions along the center line of the 15-km plume follow a pattern similar to those at 0.7 km. However, at this high altitude, since there are fewer collisions/meter the processes are stretched out over greater downstream distances.

In figures 17 and 18 are cross-sectional velocity profiles for the 0.7- and 15-km shuttle motors at several downstream stations. In figures 19 and 20 temperature profiles for these two cases are presented. At $x/r = 0$, both temperature and velocity across the exit plane are assumed to be constant and are much higher than ambient levels. As the plume gases entrain air and afterburn farther downstream, the temperature particularly along the center line rises even above the nozzle-exit plane value. Upon completion of afterburning, as dilution sets in, the plume cools so that far downstream the temperatures of the plume gases approach ambient values. The velocity of the gases is a decreasing function of downstream distance as the shear forces slow the gas molecules to ambient speeds.

Table XII contains a summary of the chemical composition of all plumes considered in this study.

CONCLUDING REMARKS

The physical, thermodynamic, and chemical properties of solid rocket motor plumes have been studied by use of an axisymmetric, time-independent model which includes the effects of turbulent mixing and finite rate chemistry. A modification has been introduced into the model to conserve mass far downstream of the exit plane.

The shuttle and Titan III-C boosters are studied. The quantity of NO produced seems to fall off rapidly with increasing altitude. Combustion is seen to be complete as nearly all the CO at the exit plane has been converted to CO_2 far downstream. Chlorine is partitioned largely between HCl and Cl_2 with 90 percent of the weight in the form of HCl.

Langley Research Center
National Aeronautics and Space Administration
Hampton, VA 23665
October 6, 1976

REFERENCES

1. Stewart, Roger B.; and Gomberg, Richard I.: The Production of Nitric Oxide in the Troposphere as a Result of Solid-Rocket-Motor Afterburning. NASA TN D-8137, 1976.

2. Mikatarian, R. R.; and Pergament, H. S.: Aerochem Axisymmetric Mixing With Nonequilibrium Chemistry Computer Program. TP-200 (Contract AF 04(611)-11541), AeroChem Res. Lab., Inc., June 1969. (Available from DDC as AD 856017.)

3. Vincenti, Walter G.; and Kruger, Charles H., Jr.: Introduction to Physical Gas Dynamics. John Wiley & Sons, Inc., c.1965.

4. Donaldson, Coleman duP.; and Gray, K. Evan: Theoretical and Experimental Investigation of the Compressible Free Mixing of Two Dissimilar Gases. AIAA J., vol. 4, no. 11, Nov. 1966, pp. 2017-2025.

5. Pergament, H. S.; and Mikatarian, R. R.: Prediction of Minuteman Exhaust Plume Electrical Properties. AFRPL-TR-72-129, U.S. Air Force, July 1973.

6. U.S. Standard Atmosphere, 1962. NASA, U.S. Air Force, and U.S. Weather Bur., Dec. 1962.

7. JANAF Thermochemical Tables. Second ed. NSRDS-NBS 37, U.S. Dep. Com., June 1971.

8. Pergament, H. S.; and Jensen, D. E.: Influence of Chemical Kinetic and Turbulent Transport Coefficients on Afterburning Rocket Plumes. J. Spacecraft & Rockets, vol. 8, no. 6, June 1971, pp. 643-649.

9. Jensen, D. E.; and Jones, G. A.: Gas-Phase Reaction Rate Coefficients for Rocketry Applications. RPE-TR-71/9, Rocket Propulsion Establishment (Westcott, England), Oct. 1971.

10. Garvin, David: Chemical Kinetics Data Survey. IV. Preliminary Tables of Chemical Data for Modelling of the Stratosphere. NBSIR 73-203, U.S. Dep. Com., May 1973.

11. Garvin, David, ed.: Chemical Kinetics Data Survey V. Sixty-Six Contributed Rate and Photochemical Data Evaluations on Ninety-Four Reactions. NBSIR 73-206, Nat. Bur. Standards, U.S. Dep. Com., May 1973.

12. Garvin, David; and Hampson, R. F., eds.: Chemical Kinetics Data Survey VII. Tables of Rate and Photochemical Data for Modelling of the Stratosphere (Revised). NBSIR 74-430, Nat. Bur. Standards, U.S. Dep. Com., Jan. 1974. (Supersedes NBSIR 73-203.)

13. Pergament, Harold S.; and Thorpe, Roger D.: NO_x Deposited in the Stratosphere by the Space Shuttle. Aero-Chem TN-161 (Contract NAS1-13544), Aero Chem Res. Labs., Inc., July 1975. (Available as NASA CR-132715.)

14. Solid Propellant Engineering Staff: Nozzle Exit Exhaust Products From Space Shuttle Boost Vehicle (November 1973 Design). Tech. Memo. 33-712 (Contract NAS 7-100), Jet Propulsion Lab., California Inst. Technol., Feb. 1, 1975. (Available as NASA CR-136747.)

15. Ting, L.; and Libby, P. A.: Remarks on the Eddy Viscosity in Compressible Mixing Flows. J. Aerosp. Sci., vol. 27, no. 10, Oct. 1960, pp. 797-798.

TABLE I.- SPACE SHUTTLE SOLID ROCKET MOTOR EXIT PLANE CONDITIONS

[This table is based on an equilibrium model. It is appropriate for a shuttle motor at 0.7 km altitude. Space shuttle data were obtained from Ben Shackleford, Marshall Space Flight Center, Mar. 1974. These data are appropriate for altitudes less than 1 km. The mass flow obtained from using these inputs is 25 percent lower than that predicted in ref. 14.]

Species	Mole fractions
AlCl	0.00003
$AlCl_2$	.00008
$AlCl_3$	.00001
AlOCl	.00002
Al_2O_3	.07975
CO	.23205
CO_2	.02120
Cl	.00225
Fe	.00011
FeCl	.00001
$FeCl_2$	.00122
H	.00556
HCl	.15442
H_2	.27812
H_2O	.14068
NO	.00001
N_2	.08401
O	.00001
OH	.00046
ClO	8.1×10^{-9}
Cl_2	6.9×10^{-7}
HO_2	1.2×10^{-10}
NO_2	5.8×10^{-12}
N_2O	8.6×10^{-11}
O_2	2.0×10^{-7}
N^2	.0000

Exit plane conditions

p, atm	0.8345
T, K	2308
M	2.779
r, m	1.810
U, m/sec	2433.8

TABLE II.- TITAN MOTOR DATA

[This table is based on an equilibrium model. It is appropriate for altitudes of approximately 1 km. In the third column, it is assumed that the injected N_2O_4 breaks down into NO and O_2.]

Exit plane species	Without thrust vector control system	With thrust vector control system (based on 50 lb/sec-motor)
CO	2.468×10^{-1}	2.452×10^{-1}
OH	9.000×10^{-5}	9.000×10^{-5}
CO_2	1.811×10^{-2}	1.811×10^{-2}
H	3.200×10^{-3}	3.200×10^{-3}
O_2	1.035×10^{-3}	1.034×10^{-3}
HO_2	5.858×10^{-11}	5.585×10^{-11}
H_2	3.157×10^{-1}	3.136×10^{-1}
H_2O	1.058×10^{-1}	1.051×10^{-1}
NO	9.000×10^{-5}	6.680×10^{-3}
NO_2	2.002×10^{-11}	2.002×10^{-11}
N	1.884×10^{-8}	1.884×10^{-8}
N_2	8.105×10^{-2}	8.051×10^{-2}
HCl	1.510×10^{-1}	1.500×10^{-1}
N_2O	1.090×10^{-8}	1.090×10^{-8}
Cl	1.150×10^{-3}	1.150×10^{-3}
Cl_2	3.293×10^{-6}	3.293×10^{-6}
ClO	2.392×10^{-8}	2.392×10^{-8}
Al_2O_3	7.680×10^{-2}	7.170×10^{-2}
O	6.959×10^{-7}	6.959×10^{-7}

Exit plane conditions

Mass flow, Mg/sec	1.84
T_e, K	1921
p_e, atm	0.702
r_e, m	1.35

TABLE III.- INITIAL CONDITIONS

[By using these inputs, the predicted mass flows agree within 10 percent with those in ref. 14 for the shuttle]

(a) Ambient conditions

Altitude, km	Vehicle	Ambient pressure, atm	Ambient temperature, K	Free-stream velocity, m/sec
0.7	Titan	0.702	300	30.48
6	Titan	.536	260	275.8
18	Titan	.0797	207	537.6
.9	Shuttle	.8345	300	30.48
5	Shuttle	.536	260	259.3
15	Shuttle	.119	216	552.2

(b) Exit plane conditions

Altitude, km	Vehicle	Effective exit radius, m	Effective exit temperature, K	Effective exit velocity, m/sec
0.7	Titan	1.35	1921	2501
6	Titan	1.35	1921	2501
18	Titan	3.63	1375	3496
.7	Shuttle	1.81	2308	2433
6	Shuttle	1.81	2308	2433
15	Shuttle	3.56	1726	2864

TABLE IV.- CHEMICAL SCHEME*

	Reaction	Rate
1.	$OH + H_2 = H_2O + H$	$4 \times 10^{-11} \exp(-5500/RT)$
2.	$H + \overline{OH} + M = H_2O + M$	$(1 \times 10^{-28})/T$
3.	$H + HCl = \overline{Cl} + H_2$	$8.8 \times 10^{-11} \exp(-4622/RT)$
4.	$CO + HO_2 = CO_2 + \overline{OH}$	$1 \times 10^{-11} \exp(-3968/RT)$
5.	$H + \overline{Cl} + M = \overline{HCl} + M$	$(3 \times 10^{-29})/T$
6.	$O + Cl + M = ClO + M$	$(1 \times 10^{-30})/T$
7.	$O + ClO = Cl + O_2$	$5.25 \times 10^{-11} \exp(-992/RT)$
8.	$HCl + OH = H_2O + \overline{Cl}$	$7.2 \times 10^{-12} \exp(-3250/RT)$
9.	$N + NO = N_2 + O$	2.7×10^{-11}
10.	$NO_2 + H = \overline{NO} + OH$	$5.8 \times 10^{-10} \exp(-1468/RT)$
11.	$\overline{ClO} + H = HCl + O$	3.0×10^{-11}
12.	$Cl + Cl + M \rightleftharpoons Cl_2 + M$	$1.6 \times 10^{-33} \exp(1600/RT)$
13.	$H + HO_2 = H_2 + O_2$	$1 \times 10^{-10} \exp(-1984/RT)$
14.	$NO + O_3 = \overline{NO_2} + O_2$	$1.5 \times 10^{-12} \exp(-2637/RT)$
15.	$CO + \overline{OH} = CO_2 + H$	$5 \times 10^{-13} \exp(-600/RT)$
16.	$O_3 + O = O_2 + O_2$	$2 \times 10^{-11} \exp(-4600/RT)$
17.	$\overline{Cl} + O_3 = ClO + O_2$	3×10^{-11}
18.	$O + \overline{HCl} = Cl + \overline{OH}$	$2.1 \times 10^{-11} \exp(-7100/RT)$
19.	$H + Cl_2 \rightleftharpoons HCl + Cl$	2.09×10^{-10}
20.	$H_2 + HO_2 = H_2O + OH$	$1.0 \times 10^{-11} \exp(-23\ 808/RT)$
21.	$\overline{NO} + \overline{ClO} \rightleftharpoons \overline{Cl} + NO_2$	1.7×10^{-11}
22.	$OH + HO_2 = O_2 + \overline{H_2O}$	2×10^{-11}
23.	$O + HO_2 = \overline{OH} + O_2$	$3 \times 10^{-11} \exp(-4960/RT)$
24.	$NO + O + M = NO_2 + M$	$4.17 \times 10^{-33} \exp(1860/RT)$
25.	$O + O + M = O_2 + M$	$(1 \times 10^{-29})/T$
26.	$OH + OH = H_2O + O$	$1 \times 10^{-11} \exp(-1000/RT)$
27.	$O + H_2 = \overline{OH} + H$	$3 \times 10^{-11} \exp(-8200/RT)$
28.	$H + O_2 = OH + O$	$3 \times 10^{-10} \exp(-16\ 500/RT)$
29.	$O + H + M = OH + M$	$(1 \times 10^{-29})/T$
30.	$CO + O + M = CO_2 + M$	$(2 \times 10^{-29})/T \exp(-4000/RT)$
31.	$H + H + M = H_2 + M$	$(1 \times 10^{-29})/T$
32.	$ClO + OH = \overline{HO_2} + Cl$	$4 \times 10^{-11} \exp(-2777/RT)$
33.	$H + O_2 + M = \overline{HO_2} + M$	$4 \times 10^{-32} \exp(992/RT)$
34.	$Cl + \overline{HO_2} = \overline{HCl} + O_2$	$1 \times 10^{-10} \exp(-1984/RT)$
35.	$H + \overline{HO_2} = OH + \overline{OH}$	$3 \times 10^{-10} \exp(-1984/RT)$
36.	$N + O_2 = NO + O$	$(1.1 \times 10^{-14})/T \exp(-6250/RT)$

*AlCl, Al_2O_3, and $AlCl_2$ are included in the plume as inert species. Reaction rate coefficients for reactions 1, 2, 5, 15, 26, 27, 28, 29, 30, and 31 are from reference 8; reactions 3, 8, 10, and 25 are from reference 13; reactions 4, 7, 11, 13, 20, 22, 23, 32, 33, 34, and 35 are from reference 9; reactions 9, 14, 24, and 36 are from reference 11; reaction 16 is from reference 10; reaction 17 is from reference 12; reactions 18, 19, and 21 were furnished by H. Hoshizaki of Lockheed Aircraft Corporation. Rates for reactions 6 and 12 are within the error bounds set by reference 9 but are lower than the forward rate recommended.

TABLE V.- MASS FLOW OF Al_2O_3

[The following table gives an indication of how closely the law of mass conservation is obeyed. Al_2O_3 is a chemically inert species in this model. The mass flow at the exit plane should equal the mass flow 1 km downstream.]

	Mass flow at exit plane, g/sec	Mass flow at 1 km downstream, g/sec
Shuttle:		
Sea level (0.7 km)	9.938×10^5	9.699×10^5
6-km altitude	9.890×10^5	9.209×10^5
10-km altitude	1.141×10^6	1.164×10^6
15-km altitude	1.240×10^6	1.245×10^6
Cl enhanced - 10-km altitude	1.141×10^6	1.089×10^6
Cl suppressed - 10-km altitude	1.141×10^6	1.086×10^6
O enhanced - 10-km altitude	1.141×10^6	1.026×10^6
O suppressed - 10-km altitude	1.141×10^6	1.053×10^6
Combustion enhanced - 10-km altitude	1.141×10^6	1.118×10^6
Ting-Libby model - 10-km altitude	1.141×10^6	1.015×10^6
Titan:		
Sea level (0.7 km)	5.204×10^5	4.989×10^5
18-km altitude	4.905×10^5	4.635×10^5

TABLE VI.- REACTION RATE CHANGES INVOLVING ATOMIC CHLORINE

[Reaction rate coefficient = $CT^n \exp(B/RT)$]

Reaction	Cl accelerated C	Cl slowed C
1. $O + HCl = Cl + OH$	2.1×10^{-11}	1.7×10^{-11}
2. $Cl + O_3 = ClO + O_2$	1.59×10^{-11}	3.09×10^{-11}
3. $HCl + OH = H_2O + Cl$	1.0×10^{-11}	4.0×10^{-12}
4. $H + HCl = Cl + H_2$	8.8×10^{-10}	8.8×10^{-12}
5. $H + Cl + M = HCl + M$	1.0×10^{-31}	1.0×10^{-27}
6. $Cl + Cl + M = Cl_2 + M$	5.0×10^{-34}	1×10^{-32}
7. $NO + ClO = Cl + NO_2$	1.9×10^{-11}	1.5×10^{-11}
8. $Cl + HO_2 = HCl + O_2$	2.0×10^{-12}	1.0×10^{-29}
9. $O + Cl + M = ClO + M$	6.6×10^{-31}	3.0×10^{-29}
10. $H + Cl_2 = HCl + Cl$	2.09×10^{-10}	1.28×10^{-10}
11. $ClO + OH = HO_2 + Cl$	4.0×10^{-10}	1.33×10^{-12}
12. $O + ClO = Cl + O_2$	5.0×10^{-10}	5.0×10^{-12}

TABLE VII.- REACTION RATE CHANGES INVOLVING ATOMIC OXYGEN

	Reaction	C for O accelerated	C for O slowed
1.	$O_3 + O = O_2 + O_2$	1.0×10^{-11}	4.0×10^{-11}
2.	$NO + O + M = NO_2 + M$	2.0×10^{-33}	8.0×10^{-33}
3.	$O + O + M = O_2 + M$	3.0×10^{-31}	3.0×10^{-28}
4.	$OH + OH = H_2O + O$	5.0×10^{-11}	2.0×10^{-12}
5.	$O + H_2 = OH + H$	9.7×10^{-12}	8.7×10^{-11}
6.	$H + O_2 = OH + O$	1.1×10^{-9}	1.2×10^{-10}
7.	$O + H + M = OH + M$	3.0×10^{-29}	3.0×10^{-28}
8.	$N + NO = N_2 + O$	5.07×10^{-11}	1.5×10^{-11}
9.	$N + O_2 = NO + O$	1.4×10^{-14}	8.3×10^{-15}
10.	$O + HCl = Cl + OH$	1.7×10^{-11}	2.2×10^{-11}
11.	$ClO + H = HCl + O$	3.0×10^{-10}	3.0×10^{-13}
12.	$O + ClO = Cl + O_2$	5.25×10^{-12}	5.0×10^{-10}
13.	$O + HO_2 = OH + O_2$	1.0×10^{-12}	9.0×10^{-10}
14.	$CO + O + M = CO_2 + M$	3.0×10^{-31}	8.0×10^{-29}
15.	$O + Cl + M = ClO + M$	6.66×10^{-31}	3.0×10^{-29}

TABLE VIII.- REACTION RATE CHANGES INVOLVING COMBUSTION

[All other reactions are the same as in table IV.
Rate = $CT^n \exp(B/RT)$]

	Reaction	C for combustion accelerated
1.	$OH + H_2 = H_2O + H$	4.0×10^{-11}
2.	$OH + OH = H_2O + O$	5.0×10^{-11}
3.	$O + H_2 = OH + H$	8.7×10^{-11}
4.	$H + O_2 = OH + O$	1.1×10^{-9}
5.	$H + H + M = H_2 + M$	1.5×10^{-27}
6.	$H + O + M = OH + M$	3.0×10^{-28}
7.	$H + OH + M = H_2O + M$	2.0×10^{-27}
8.	$O + O + M = O_2 + M$	3.0×10^{-28}
9.	$CO + OM = CO_2 + M$	5.4×10^{-13}
10.	$CO + O + M = CO_2 + M$	8.0×10^{-29}

TABLE IX.- NO_x PRODUCTION (AT 1 km DOWNSTREAM FROM EXIT)

	NO, g/m	NO_2, g/m
Shuttle:		
Sea level (0.7 km)	1052	12.88
6-km altitude	116	1.5
10-km altitude	25	.48
15-km altitude	6	.14
Cl enhanced - 10-km altitude	29	.166
Cl suppressed - 10-km altitude	37	.82
O enhanced - 10-km altitude	30	.82
O suppressed - 10-km altitude	20	
Combustion enhanced - 10-km altitude	32	.64
Ting-Libby model - 10-km altitude	41	.20
Titan:		
Sea level (0.7 km)	489.6	6.34
18-km altitude	21.7	.12

TABLE X.- CHLORINE PARTITIONING PERCENT BY WEIGHT OF REACTING COMPOUNDS CONTAINING CHLORIDE AT 1 km DOWNSTREAM

	HCl	Cl_2	Cl	ClO
Shuttle:				
Sea level (0.7 km)	89.75	10.10	0.14	0.01
6-km altitude	88.69	10.68	.62	.01
10-km altitude	85.54	12.65	1.80	.01
15-km altitude	78.06	15.13	6.80	.11
Cl enhanced* - 10-km altitude	83.91	11.71	4.37	.02
Cl suppressed* - 10-km altitude	84.67	14.70	.62	.03
O enhanced - 10-km altitude	86.74	11.22	2.02	.01
O suppressed* - 10-km altitude	84.34	13.93	2.14	0
Combustion enhanced* - 10-km altitude	84.55	13.27	2.17	.01
Ting-Libby model - 10-km altitude	92.49	7.11	.45	0
Titan:				
Sea level (0.7 km)	89.90	9.90	.20	0
19-km altitude	74.56	12.35	13.12	.01

*Plume reactions are still occurring, these numbers will change further downstream.

TABLE XI.- CARBON PARTITIONING

	CO at exit plane, g/m	CO_2 at exit plane, g/m	CO (x = 1 km), g/m	CO_2, g/m
Shuttle:				
Sea level (0.7 km)	356	51	50.5	29 828
6-km altitude	334	48	17	4 371
10-km altitude	312	45	39.5	3 283
15-km altitude	319	45	37	2 705
Cl enhanced - 10-km altitude	312	45	22	3 285
Cl suppressed - 10-km altitude	312	45	30	3 262
O enhanced - 10-km altitude	312	45	18	3 083
O suppressed - 10-km altitude	312	45	21	3 176
Combustion enhanced - 10-km altitude	312	45	26	3 358
Ting-Libby model - 10-km altitude	312	45	13	2 942
Titan:				
Sea level (0.7 km)	213	25	38	17 698
18-km altitude	173	21	18	1 212

TABLE XII.- AMOUNT OF COMPOUNDS

	Amount of certain compounds 1 km downstream of exit plane, g/m					
	Titan, 0.9 km	Titan, 18 km	Shuttle, 0.7 km	Shuttle, 6 km	Shuttle, 10 km	Shuttle, 15 km
HCl	7 565	466	13 708	1992	1420	1099
Cl_2	833	77.2	1 543	240	210	213
ClO	.05	.075	.5	.070	.04	.16
Cl	16.7	82	21.6	14	30	95.8
NO	489	22	954	107	28	5.7
NO_2	6.3	.12	12.9	1.5	.4	.13
CO	38.3	18	50	17	25	37.6
CO_2	17 698	1212	29 828	4372	3274	2705
Al_2O_3	11 194	781	21 807	3205	2418	2018
H_2	.006	.0053	.02	.002	.006	.005
H_2O	11 791	838	20 713	3055	2320	1959
O	.0003	.097	.0002	.0005	.005	.12
OH	.003	.073 (Still reacting)	.004	.002	.008	.11 (Still reacting)

TABLE XII.- Concluded

	Amount of certain compounds 1 km downstream of the exit plane, g/m for 10-km shuttle with parameter variations					
	Cl reactions faster	Cl reactions slower	O reactions faster	O reactions slower	Combustion faster	Ting-Libby
HCl	1419	1428	1376	1379	1465	1391
Cl_2	198	248	178	221	230	107
ClO	.04	.05	.15	.04	.18	.002
Cl	74	10.5	32	35	37.6	6.7
NO	29	37	30	20	32	40.9
NO_2	.16	.8	.8	.17	.64	.19
CO^2	22	30	17	21	26.5	12.8
CO_2	3285	3262	3084	3176	3358	2942
$Al_2^2O_3$	2420	2412	2268	2339	2478	2146
H_2	.002	.008	.000	.000	.005	.000
H_2^2O	2324	2314	2167	2244	2377	2029
O^2	.01	.001	.005	.002	.007	.000
OH	.03	.003	.009	.010	.014	.000 (Still reacting)

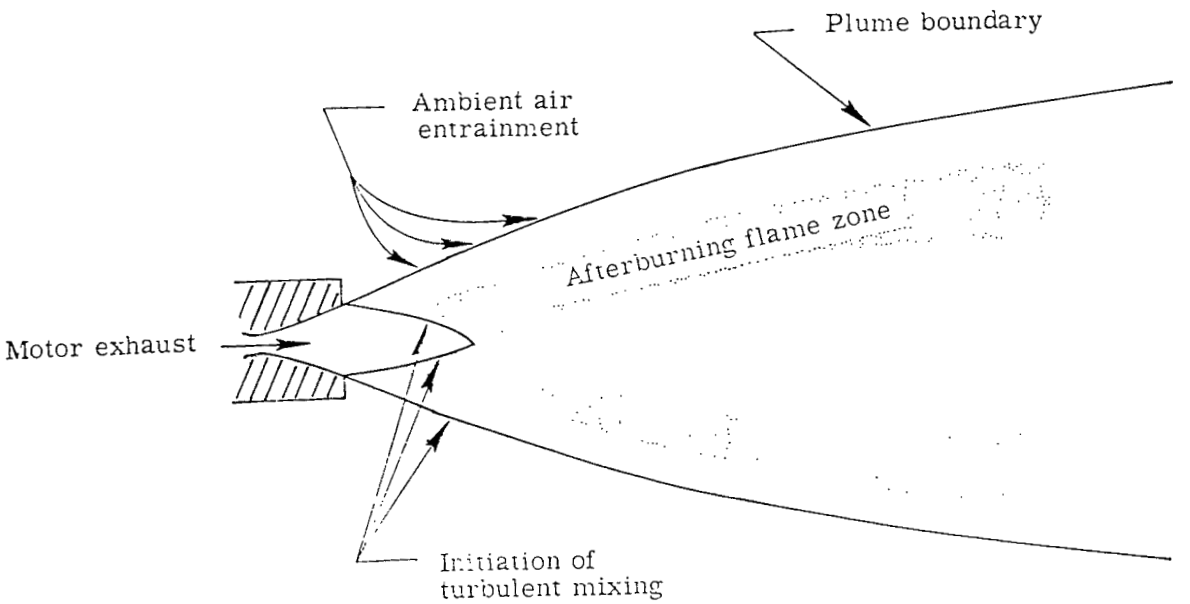

Figure 1.- Physical processes of afterburning.

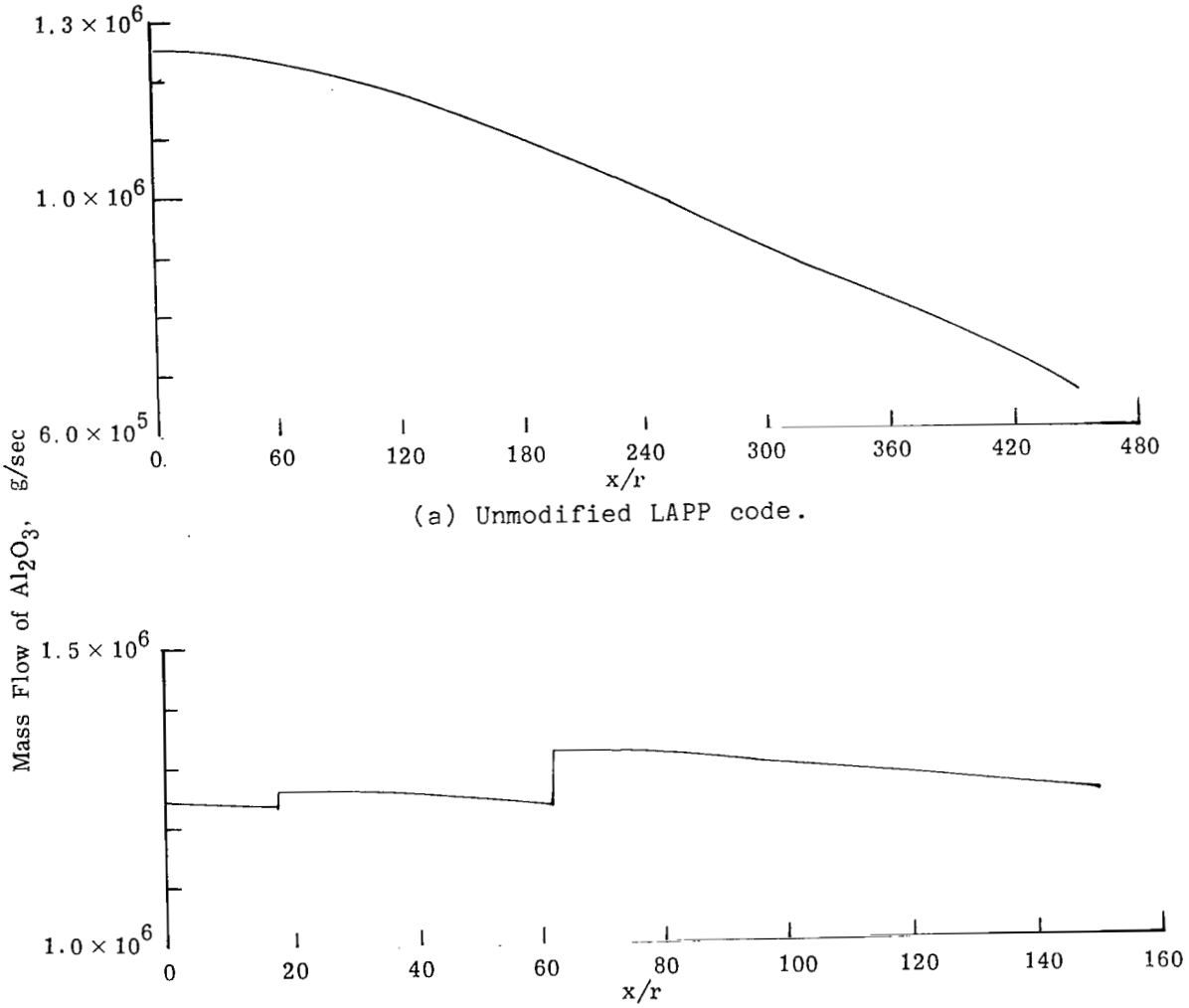

Figure 2.- Predicted mass flow of Al_2O_3 as a function of downstream in distance in plume of a shuttle motor at an altitude of 15 km for unmodified and modified LAPP code.

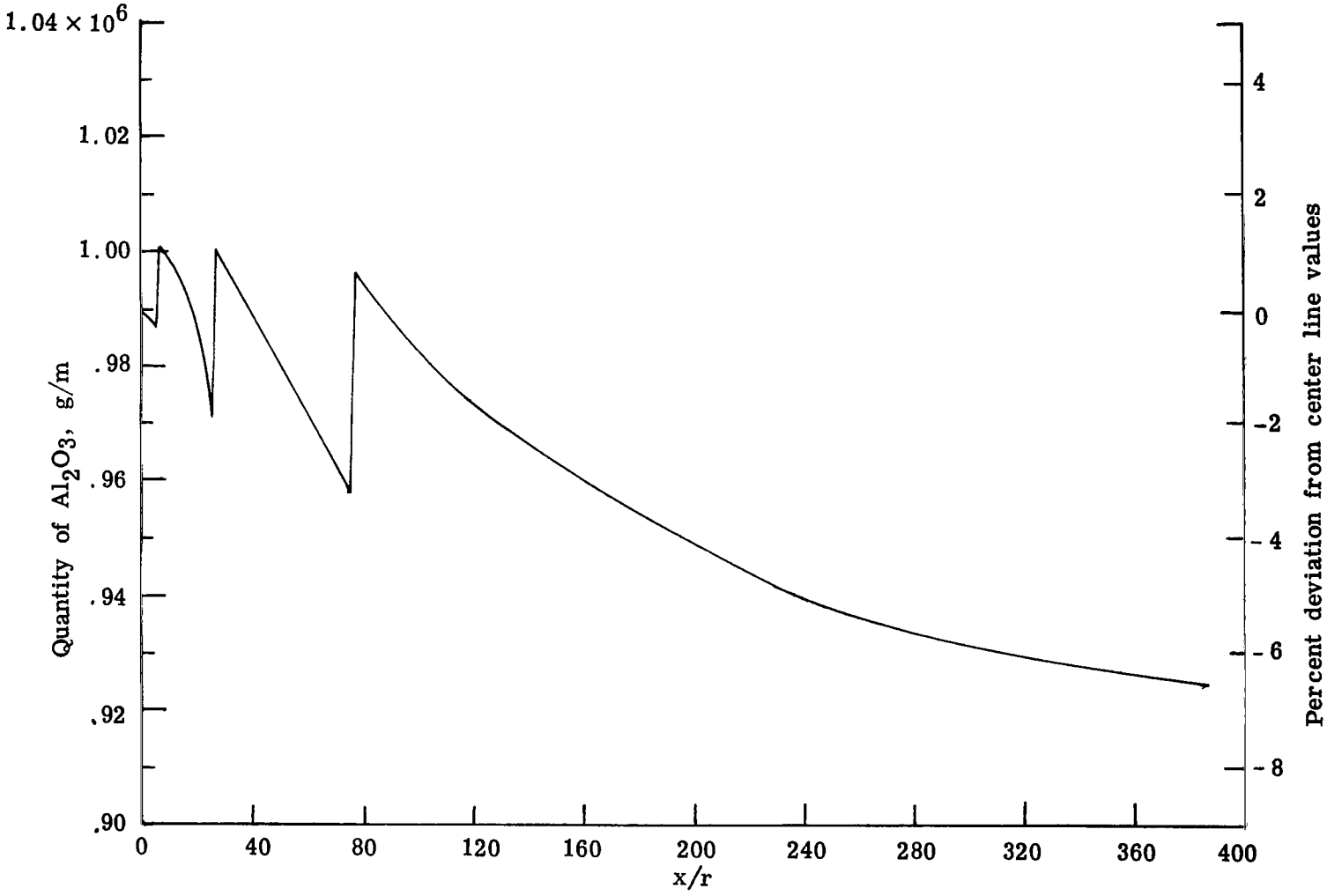

Figure 3.- Mass flow of Al_2O_3 as a function of downstream distance in plume of a shuttle motor at an altitude of 5 km.

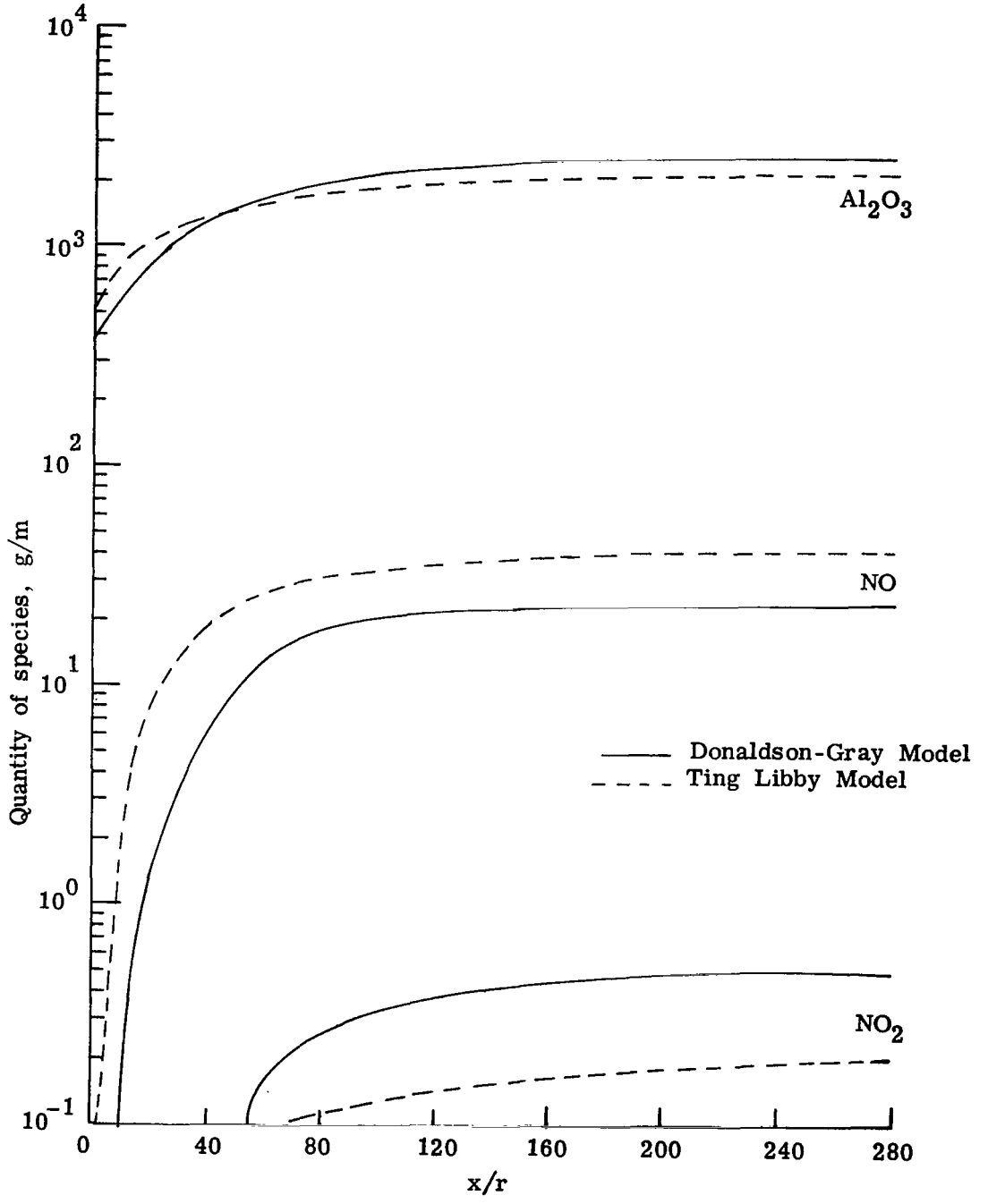

Figure 4.- Production of NO_x as a function of downstream distance in plume of a shuttle motor at an altitude of 10 km by using Donaldson-Gray and and Ting-Libby eddy-viscosity models.

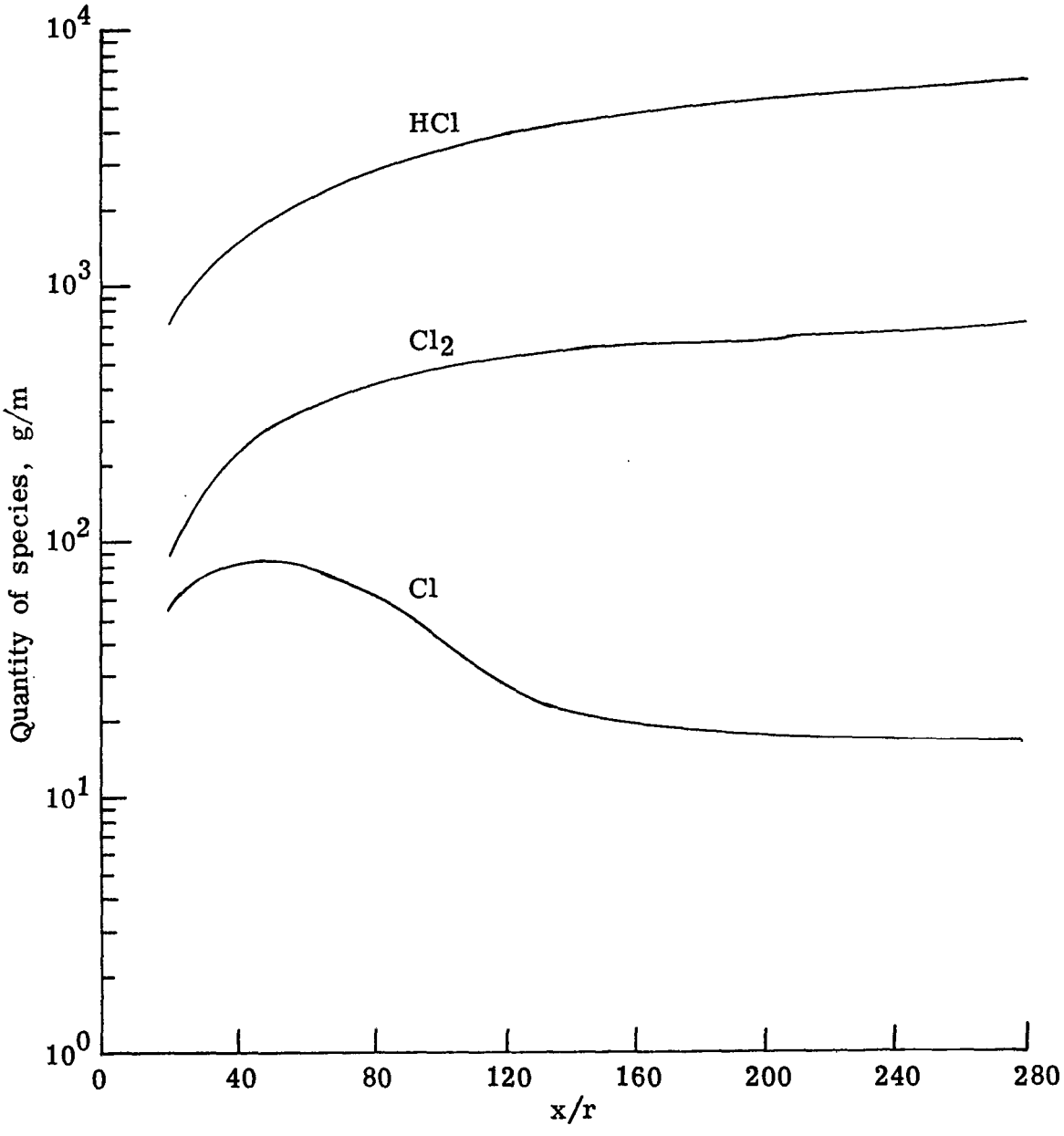

Figure 5.- Quantity of several chlorine containing species as a function of downstream distance in plume of a Titan motor at an altitude of 0.9 km.

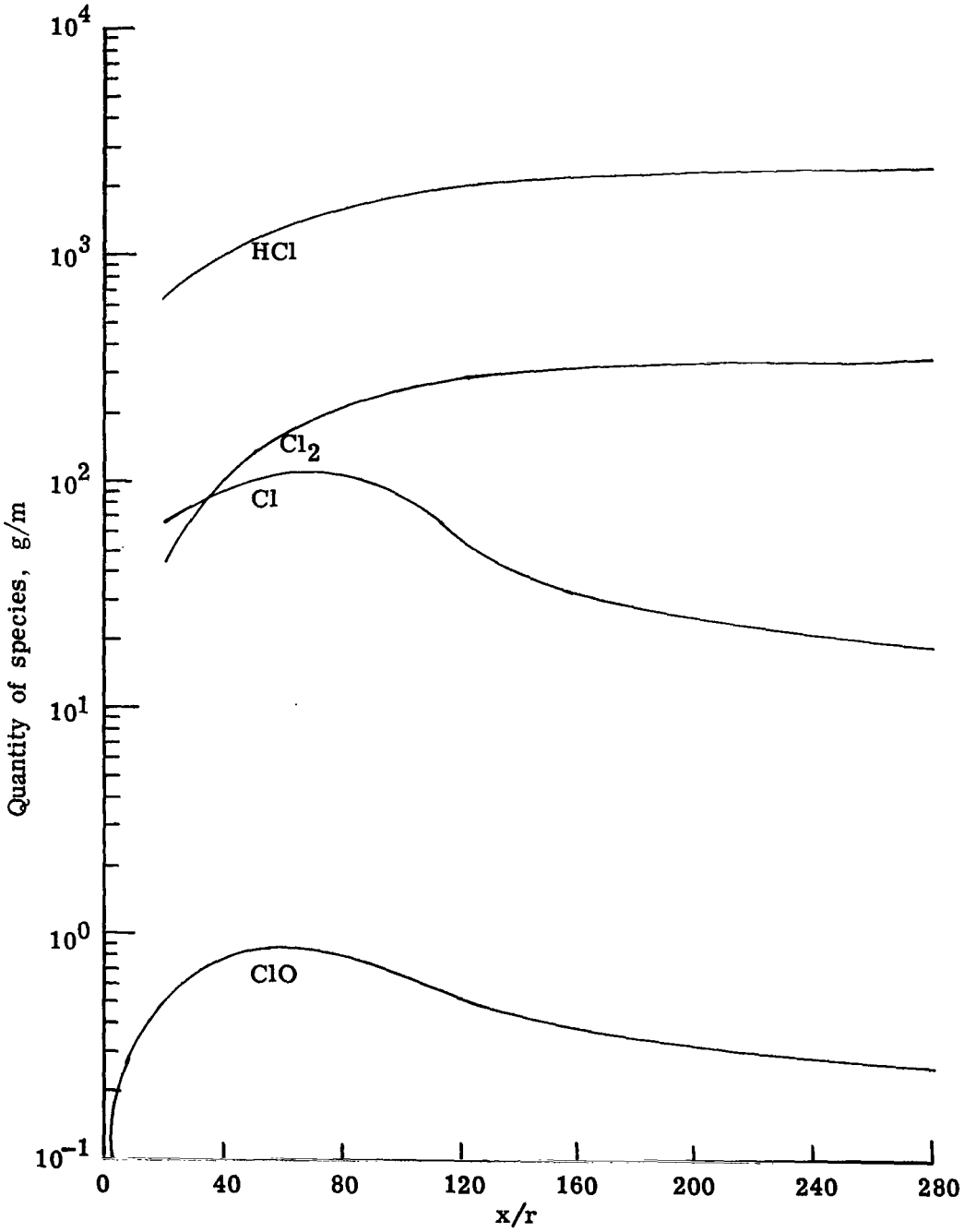

Figure 6.- Quantity of several chlorine containing species as a function of downstream distance in plume of a shuttle motor at an altitude of 5 km.

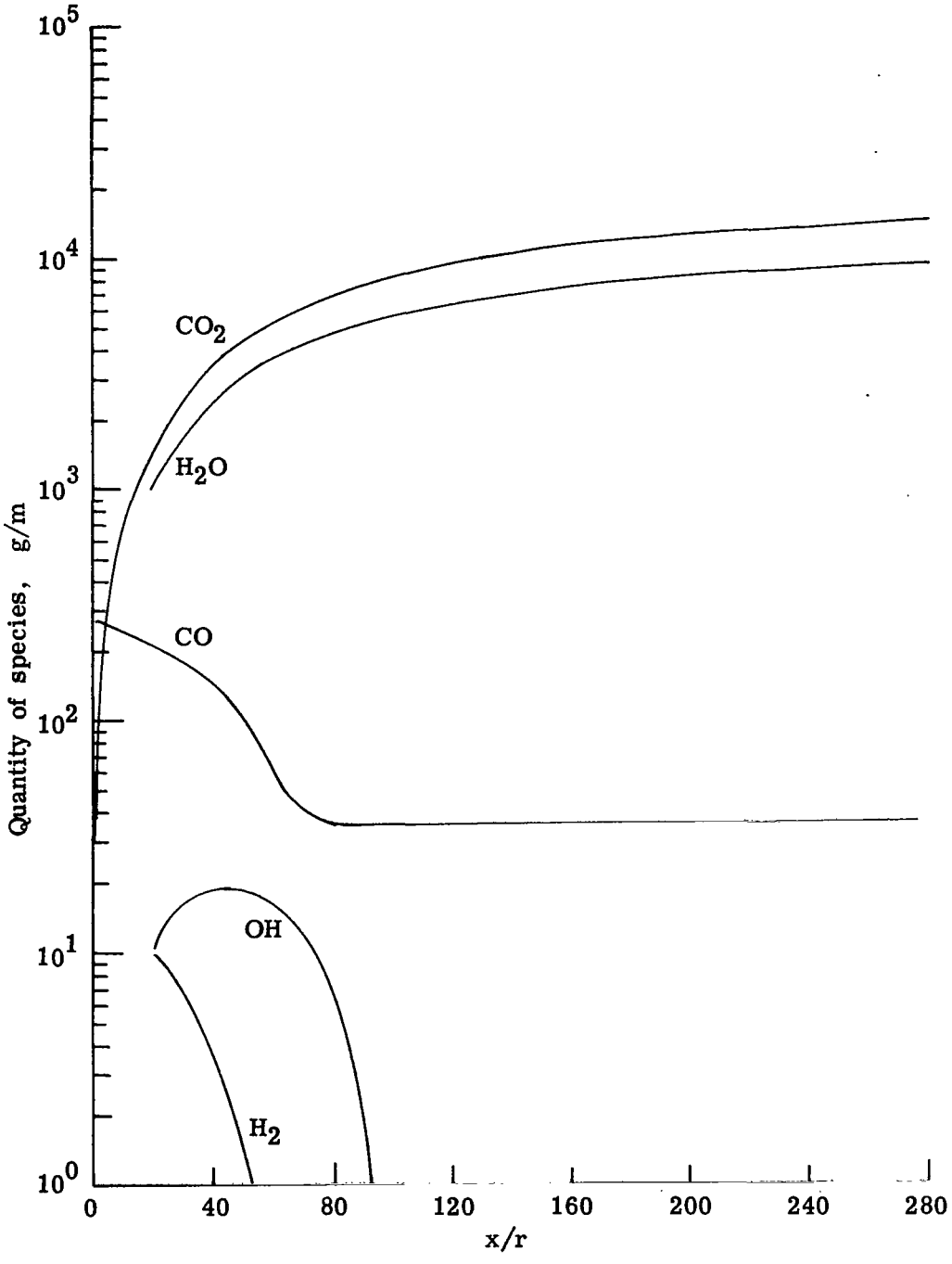

Figure 7.- Quantity of several species related to combustion processes as a function of downstream distance in plume of a Titan motor at 0.9 km.

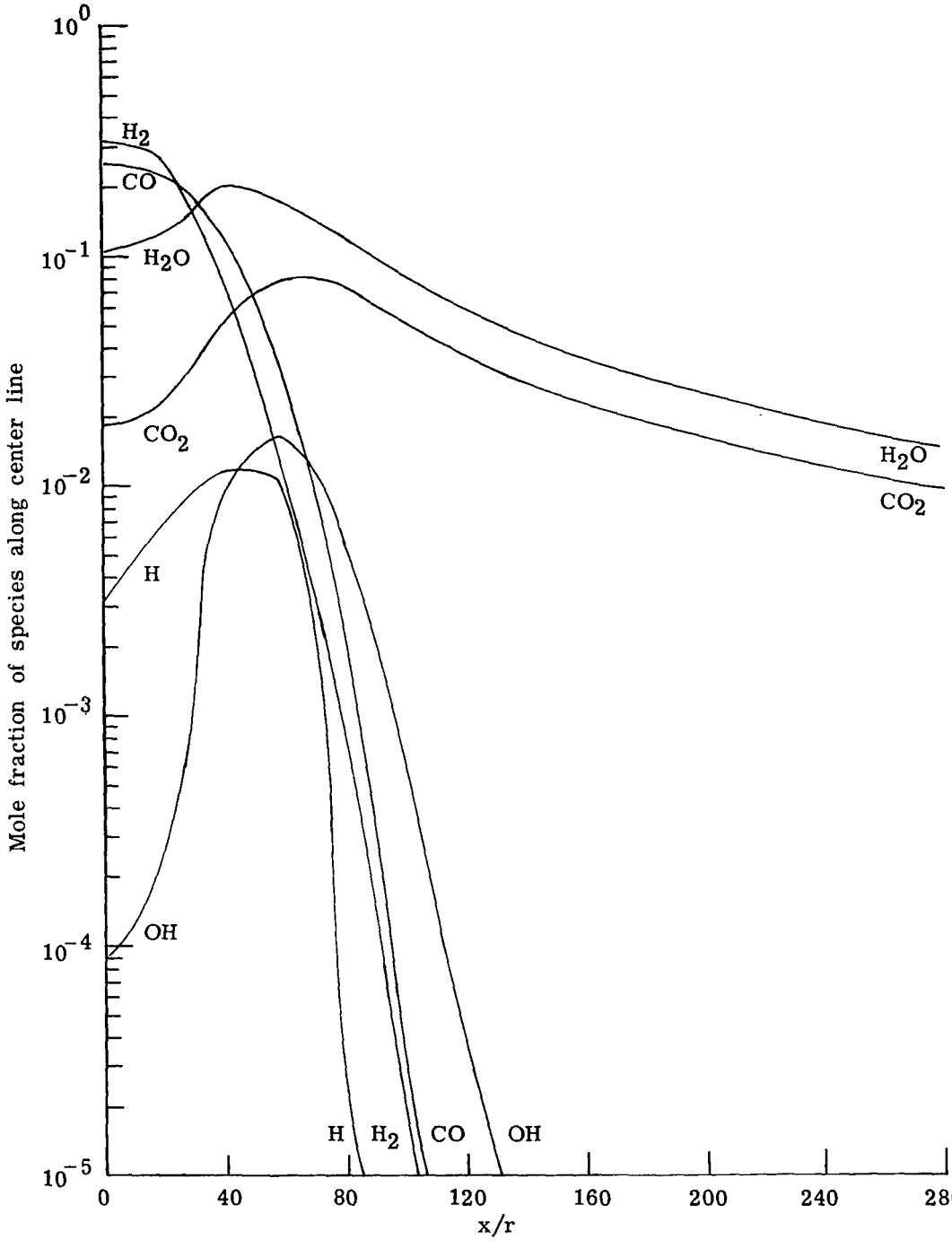

Figure 8.- Mole fractions along center line of several species related to combustion processes as a function of downstream distance in plume of a Titan motor at 0.9 km.

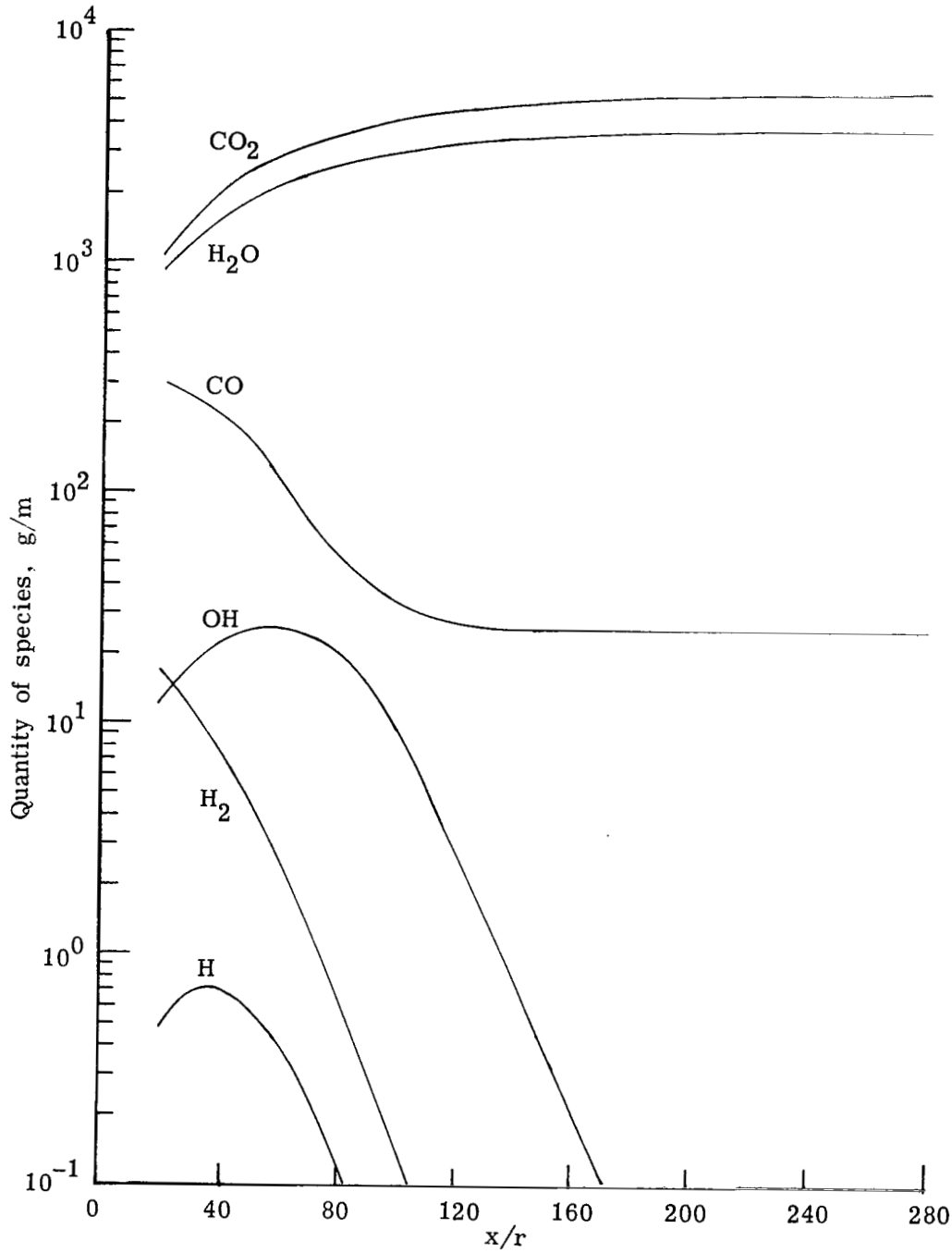

Figure 9.- Quantity of several species related to combustion processes as a function of downstream distance in plume of a shuttle motor at an altitude of 6 km.

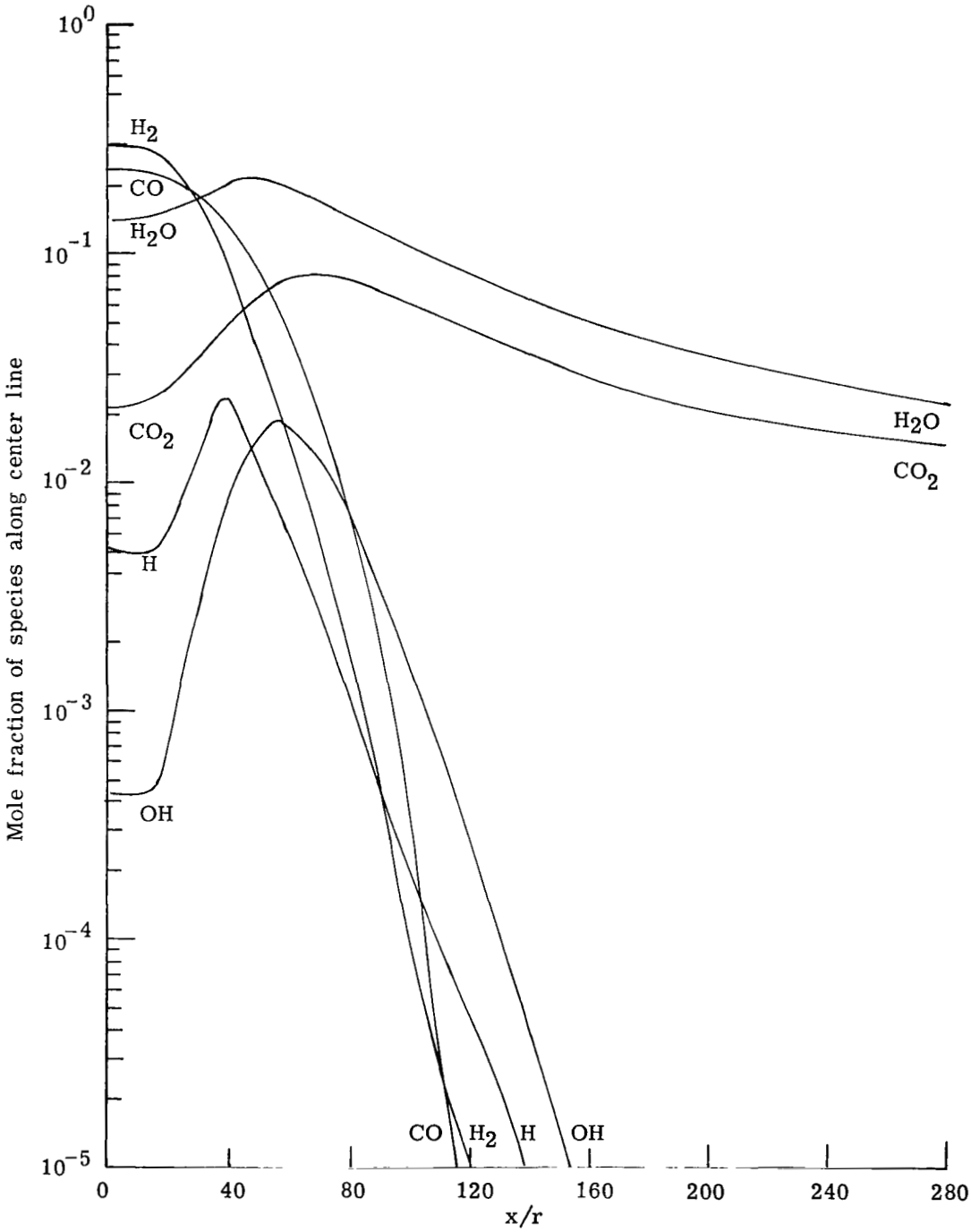

Figure 10.- Mole fractions along center line of several species related to combustion processes as a function of downstream distance in plume of a shuttle motor at an altitude of 6 km.

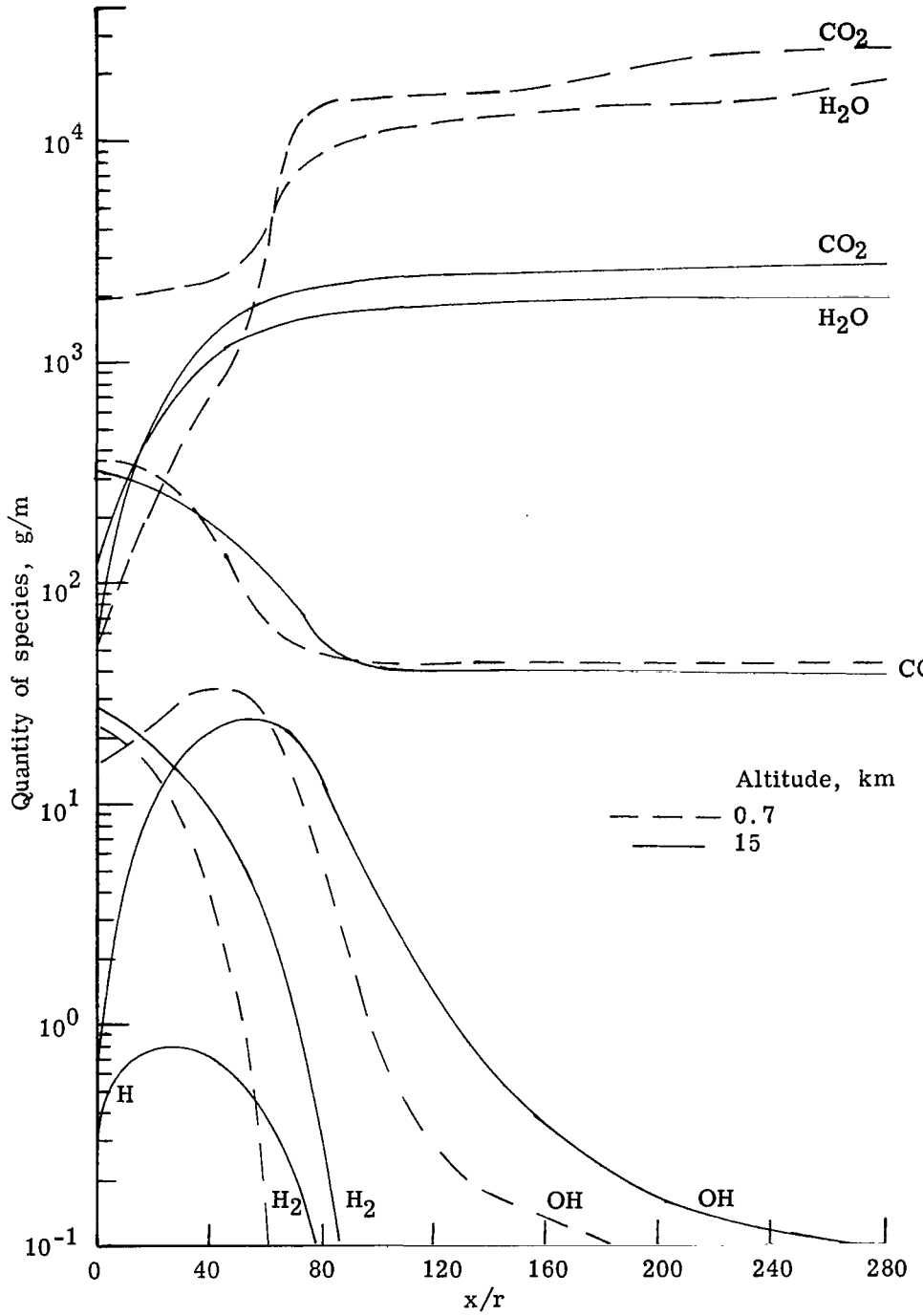

Figure 11.- Quantity of several species related to combustion processes as a function of downstream distance in plume of a shuttle motor at altitudes of 0.7 km and 15 km.

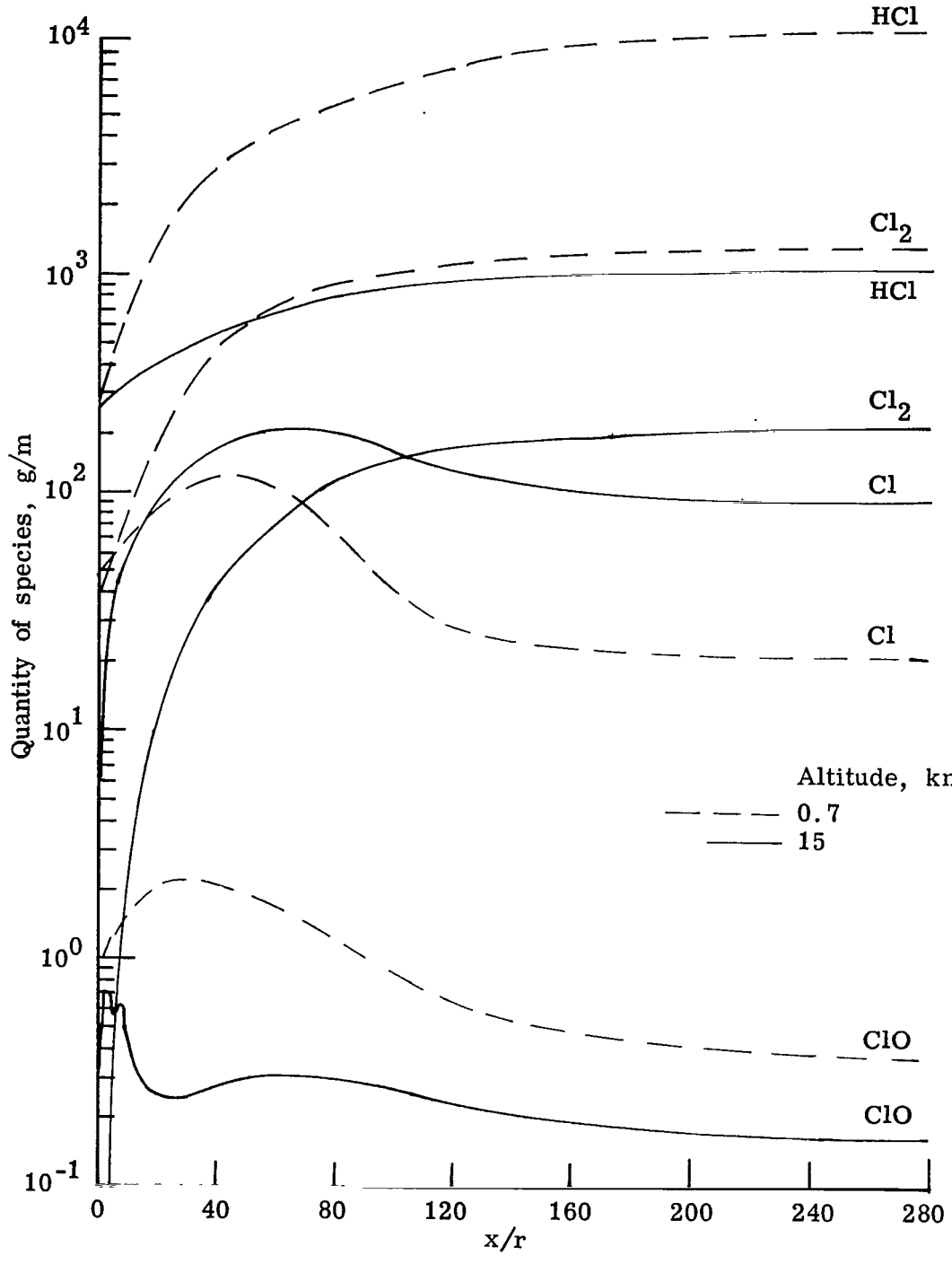

Figure 12.- Quantity of several species containing chlorine as a function of downstream distance in plume of a shuttle motor at altitudes of 0.7 km and 15 km.

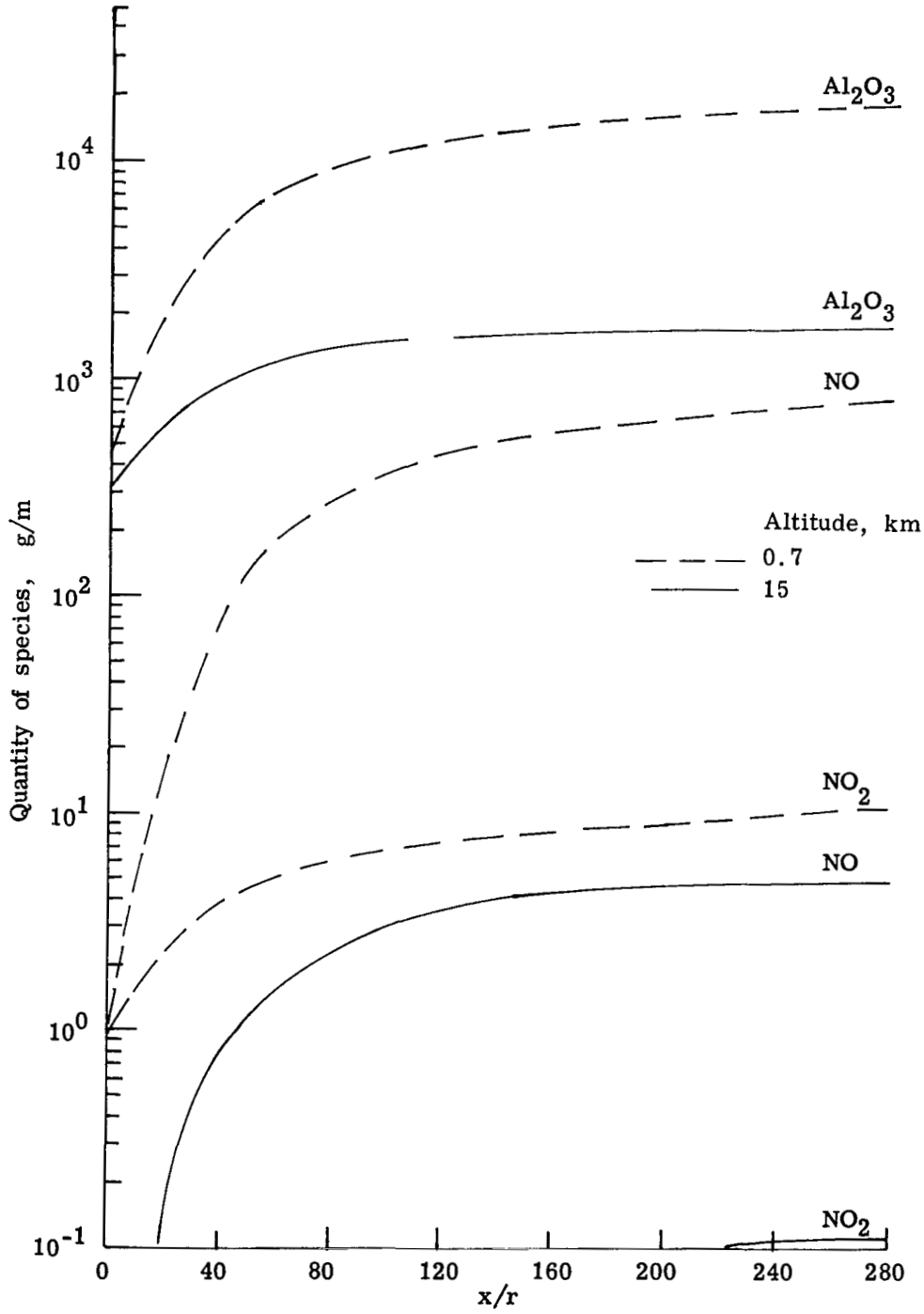

Figure 13.- Quantity of NO_x as a function of downstream distance in plume of a shuttle motor at altitudes of 0.7 km and 15 km.

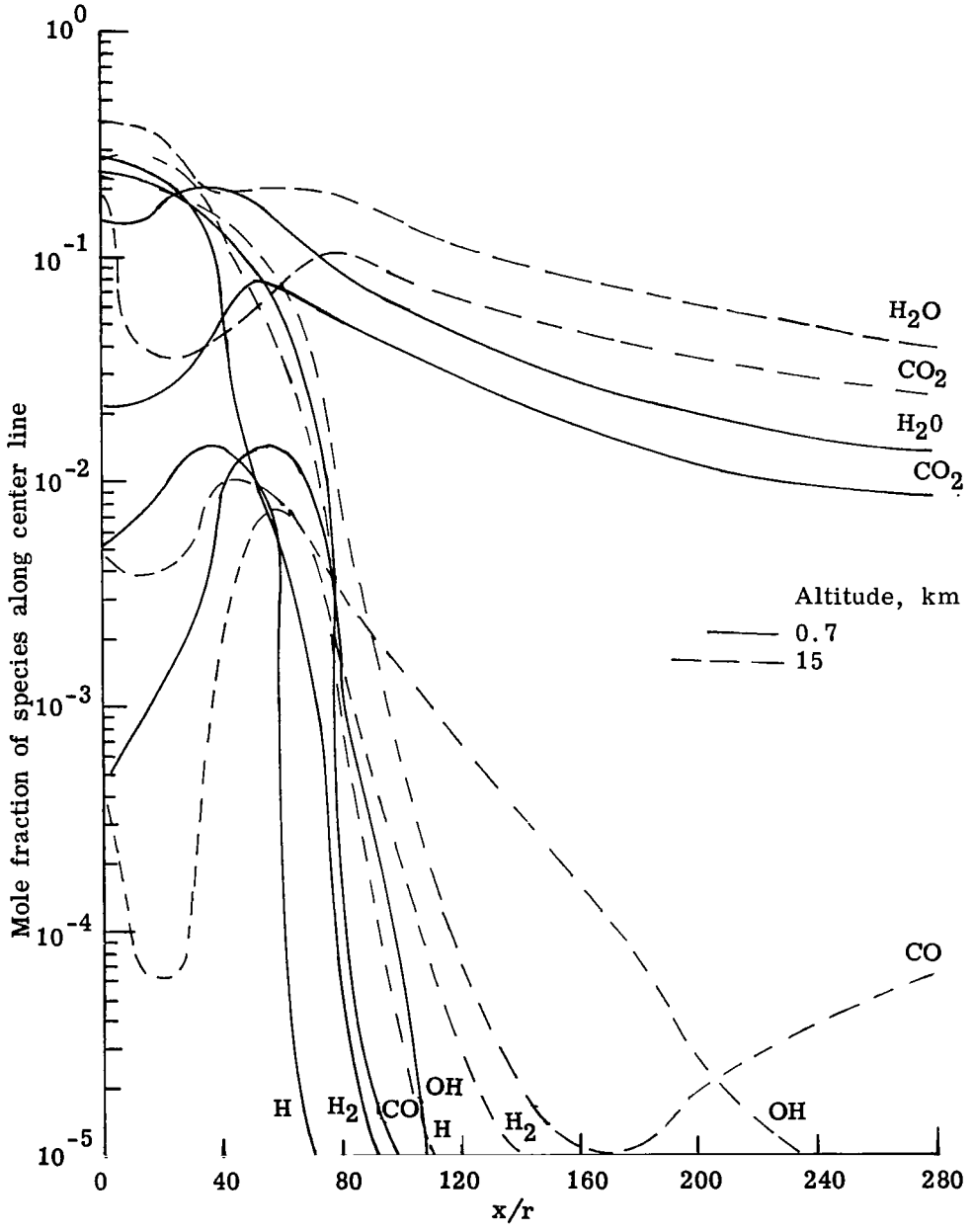

Figure 14.- Mole fractions along center line of several species related to combustion processes as a function of downstream distance in plume of a shuttle motor at altitudes of 0.7 km and 15 km.

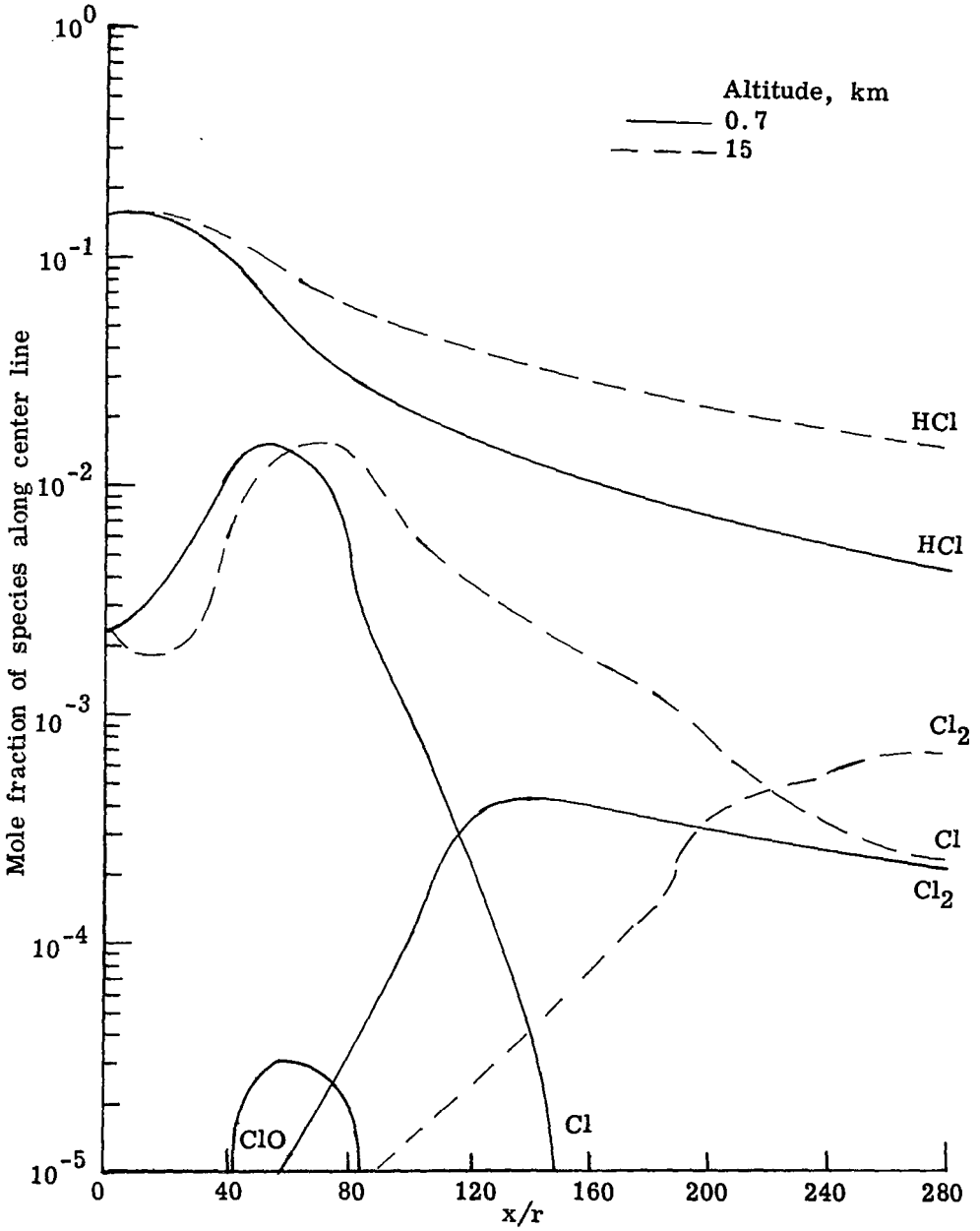

Figure 15.- Mole fractions along center line of several species containing chlorine as a function of downstream distance in plume of a shuttle motor at altitudes of 0.7 km and 15 km.

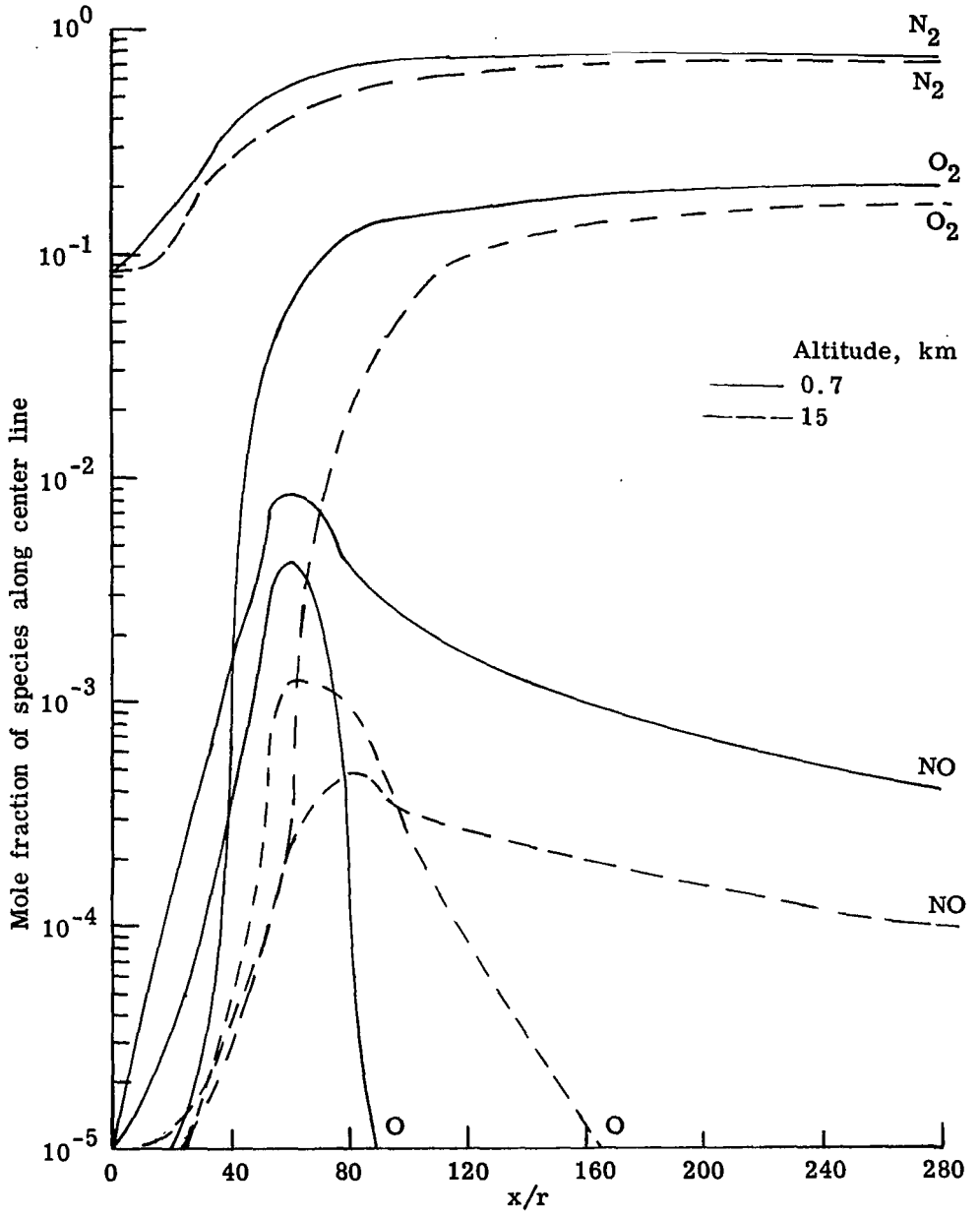

Figure 16.- Mole fractions along center line of several species related to NO as a function of downstream distance in plume of a shuttle motor at altitudes of 0.7 km and 15 km.

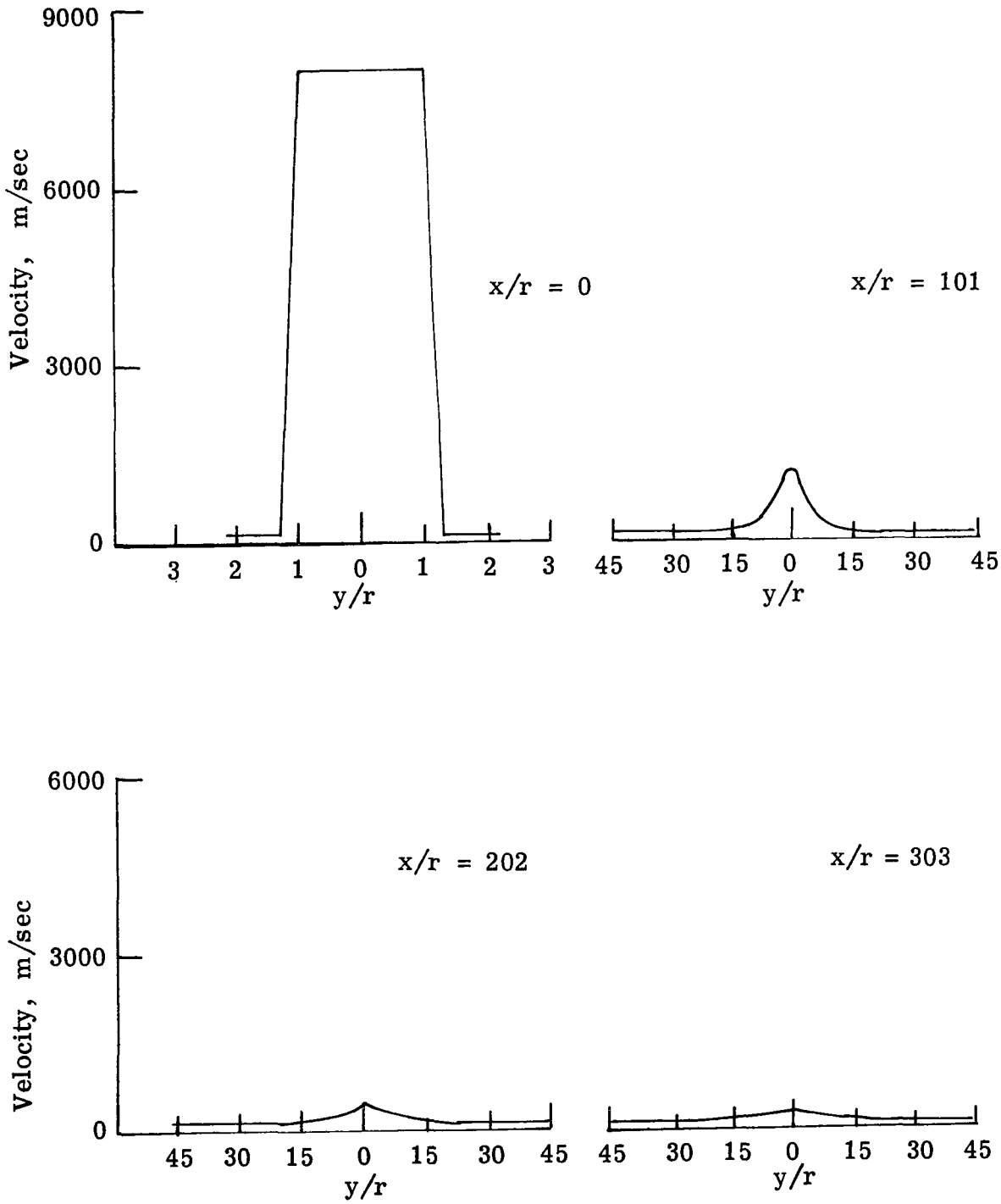

Figure 17.- Velocity profiles at several downstream stations in plume of a shuttle motor at an altitude of 0.7 km.

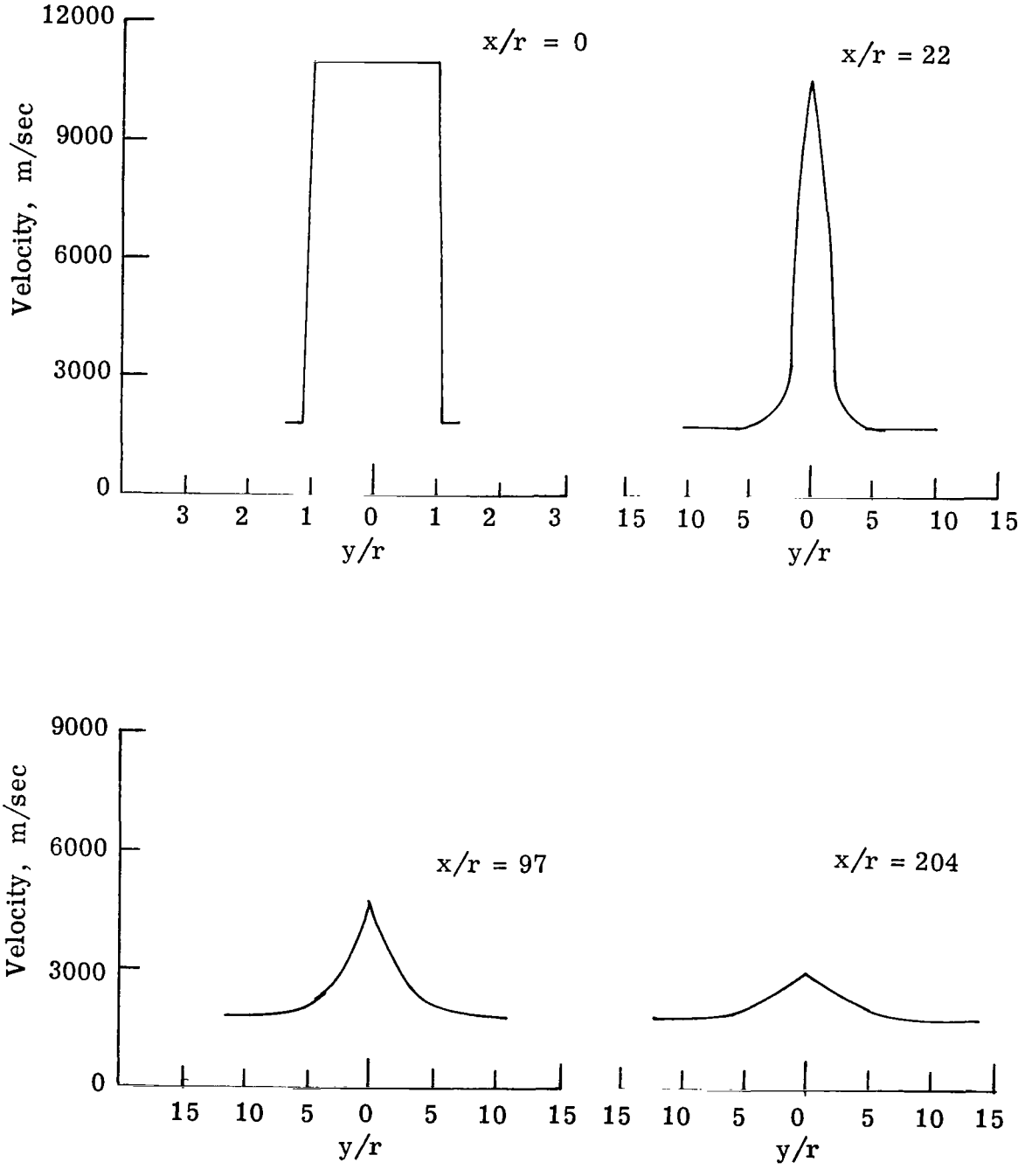

Figure 18.- Velocity profiles at several downstream stations in plume of a shuttle motor at an altitude of 15 km.

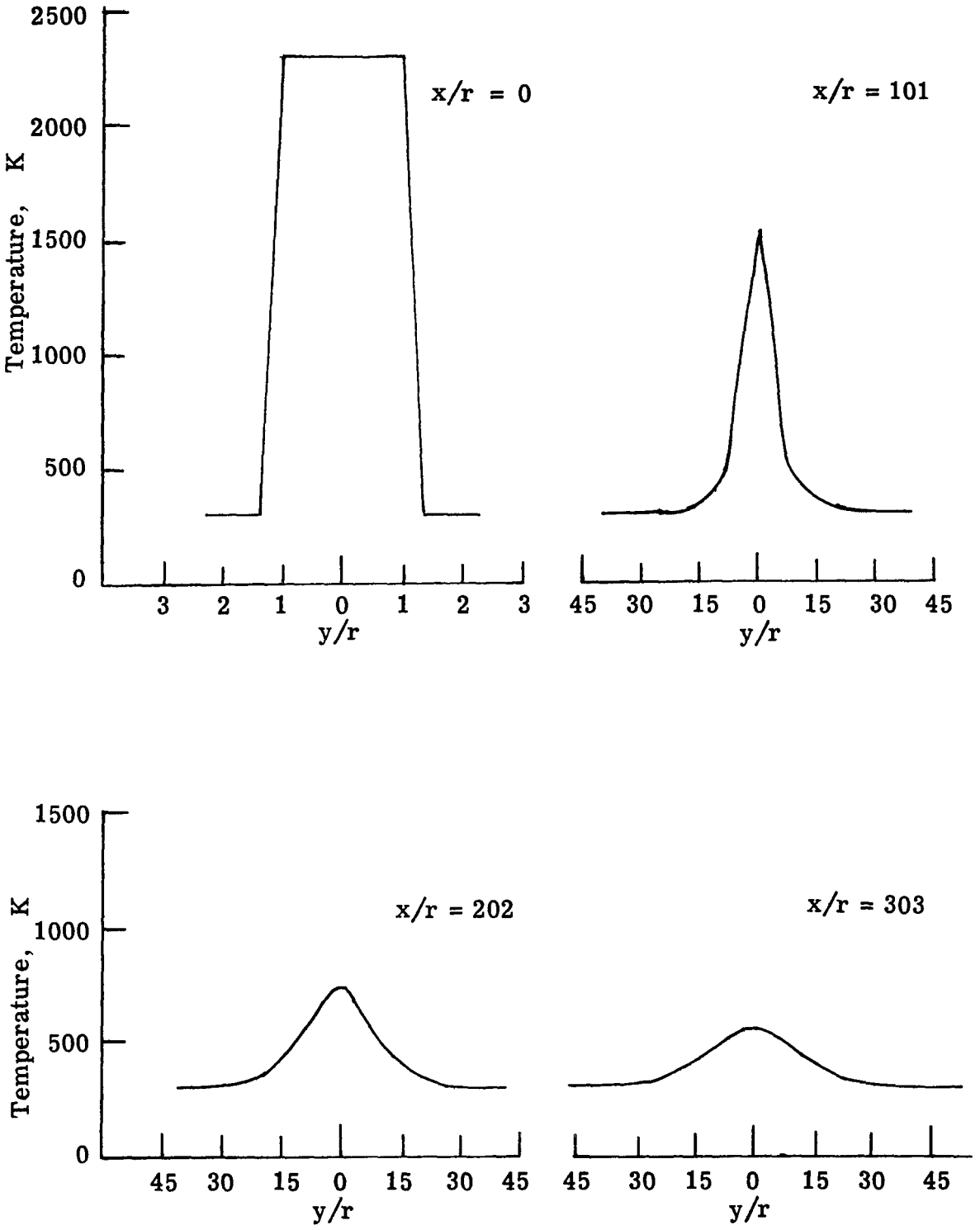

Figure 19.- Temperature profiles at several downstream stations in plume of a shuttle motor at an altitude of 0.7 km.

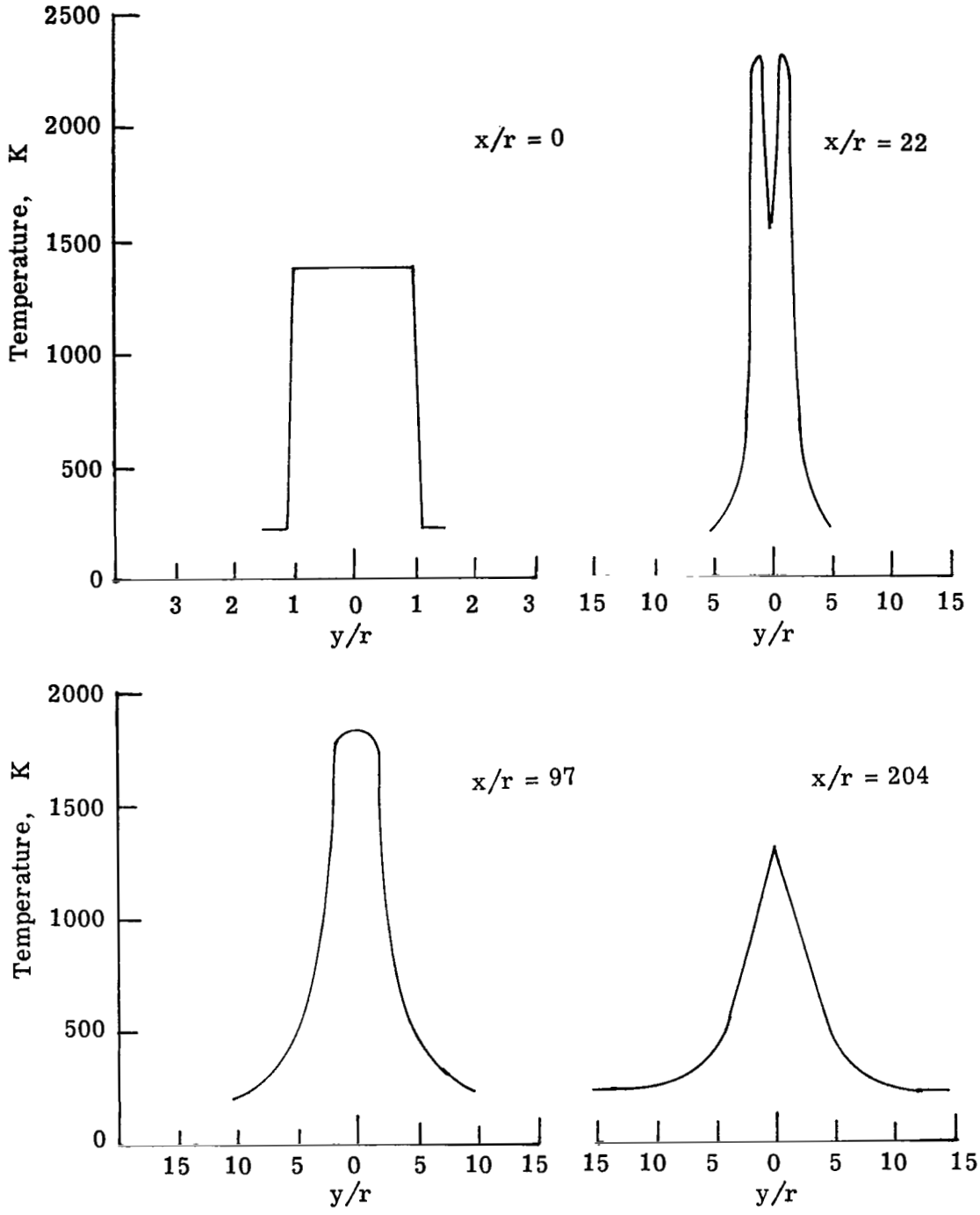

Figure 20.- Temperature profiles at several downstream stations in plume of a shuttle motor at an altitude of 15 km.

"The aeronautical and space activities of the United States shall be conducted so as to contribute . . . to the expansion of human knowledge of phenomena in the atmosphere and space. The Administration shall provide for the widest practicable and appropriate dissemination of information concerning its activities and the results thereof."

—NATIONAL AERONAUTICS AND SPACE ACT OF 1958

NASA SCIENTIFIC AND TECHNICAL PUBLICATIONS

TECHNICAL REPORTS: Scientific and technical information considered important, complete, and a lasting contribution to existing knowledge.

TECHNICAL NOTES: Information less broad in scope but nevertheless of importance as a contribution to existing knowledge.

TECHNICAL MEMORANDUMS: Information receiving limited distribution because of preliminary data, security classification, or other reasons. Also includes conference proceedings with either limited or unlimited distribution.

CONTRACTOR REPORTS: Scientific and technical information generated under a NASA contract or grant and considered an important contribution to existing knowledge.

TECHNICAL TRANSLATIONS: Information published in a foreign language considered to merit NASA distribution in English.

SPECIAL PUBLICATIONS: Information derived from or of value to NASA activities. Publications include final reports of major projects, monographs, data compilations, handbooks, sourcebooks, and special bibliographies.

TECHNOLOGY UTILIZATION PUBLICATIONS: Information on technology used by NASA that may be of particular interest in commercial and other non-aerospace applications. Publications include Tech Briefs, Technology Utilization Reports and Technology Surveys.

Details on the availability of these publications may be obtained from:

SCIENTIFIC AND TECHNICAL INFORMATION OFFICE

NATIONAL AERONAUTICS AND SPACE ADMINISTRATION

Washington, D.C. 20546